Kel1 is a phosphorylation-regulated noise suppressor of the pheromone signaling pathway

by

Ignacio Garcia[1,2], Sara Munoz[1,2], Pierre Chymkowitch[3,4], Manolis Papamichos-Chronakis[5], Aram N. Andersen[1,2,3], Christine Zimmermann[6], Jens Eriksson[7], Jorrit M. Enserink[1,2,3,*]

[1] Department of Molecular Cell Biology, Institute for Cancer Research, The Norwegian Radium Hospital, Montebello, 0379 Oslo, Norway

[2] Centre for Cancer Cell Reprogramming, Institute of Clinical Medicine, Faculty of Medicine, University of Oslo, Oslo, Norway

[3] Section for Biochemistry and Molecular Biology, Faculty of Mathematics and Natural Sciences, University of Oslo, Oslo, Norway

[4] Department of Microbiology, Oslo University Hospital

[5] Department of Molecular Physiology and Cell Signalling Institute of Systems, Molecular and Integrative Biology University of Liverpool, UK

[6] Institute for Virology, University Medical Center of the Johannes Gutenberg-University, Mainz, Germany

[7] Department of Medical Biochemistry and Microbiology, Uppsala University, Sweden

[*] To whom correspondence should be addressed: jorrit.enserink@rr-research.no

Abstract

Mechanisms have evolved that allow cells to detect signals and generate an appropriate response. The accuracy of these responses relies on the ability of cells to discriminate between signal and noise. How cells filter noise in signaling pathways is not well understood. We have analyzed noise suppression in the yeast pheromone signaling pathway. By combining synthetic genetic array screening, mass spectrometry and single-cell time-resolved microscopy, we discovered that the poorly characterized protein Kel1 serves as a major noise suppressor of the pathway. At the molecular level, Kel1 suppresses spontaneous activation of the pheromone response by inhibiting membrane recruitment of Ste5 and Far1. Kel1 is regulated by phosphorylation, and only the hypophosphorylated form of Kel1 suppresses signaling, reduces noise and prevents pheromone-associated cell death. Our data indicate that in response to pheromone the MAPKs Fus3 and Kss1 phosphorylate Kel1 to relieve inhibition of the pheromone pathway. Taken together, Kel1 serves as a phospho-regulated suppressor of the pheromone pathway to reduce noise, inhibit spontaneous activation of the pathway, regulate mating efficiency and to prevent pheromone-associated cell death.

Introduction

A crucial aspect of any organism's well-being is the ability of cells to respond to changes in their internal and external environment. Accurate signal-noise discrimination is particularly important during conditions that threaten cellular homeostasis, or when a given signal triggers cellular commitment, such as differentiation. Low levels of noise within a population of cells may be beneficial under certain conditions, by allowing a fraction of cells to survive a dramatic change in environmental conditions (Kaern et al., 2005). However, high noise levels may be detrimental to cellular fitness and has been evolutionarily minimized (Balazsi et al., 2011; Lehner, 2008; Metzger et al., 2015; Wang and Zhang, 2011). Noise has been best studied at the level of gene expression, where it is often referred to as the stochastic variation in the protein expression level of a gene among isogenic cells in a homogenous environment (Raser and O'Shea, 2005; Wang and Zhang, 2011). Gene expression noise can arise from intrinsic and extrinsic variations (Raser and O'Shea, 2005). Intrinsic noise is caused by inherent stochastic events in biochemical processes that can occur at various levels during gene expression, such as transcriptional initiation, mRNA degradation, translational initiation, and protein degradation, as well as during signal transduction (Raser and O'Shea, 2005). Extrinsic noise is caused by differences among cells, either in their local environment or the concentration or activity of any factor that influences gene expression (Raser and O'Shea, 2005; Volfson et al., 2006), such as age, cell cycle stage, metabolic state, and the number and quality of proteins and organelles distributed to the mother and daughter cell during cell division.

The yeast mating pathway is a model system for signal transduction and cellular decision-making (Alvaro and Thorner, 2016; Paliwal et al., 2007). In haploid yeast cells, this pathway detects and transmits a pheromone signal emitted by cells of the opposite mating type to induce a mating response (Fig. 1A). Activation of this pathway results in cell cycle

arrest, activation of a transcriptional program and cell wall remodeling to execute the morphological changes required to mate (Alvaro and Thorner, 2016). Given the potential fitness cost associated with inappropriate activation of this pathway (Banderas et al., 2016), pathway activation occurs in normal cells in a switch-like manner with high precision and overall low intrinsic noise (Dixit et al., 2014a; Malleshaiah et al., 2010). The pathway is activated by binding of pheromone to its G protein-coupled target receptor, resulting in dissociation of the heterotrimeric G protein into the α-subunit (Gpa1) and a Gβγ heterodimer (Ste4–Ste18)(Fig. 1A). The Gβγ complex recruits Far1 and the scaffold protein Ste5 to the plasma membrane. Membrane localization of Ste5 results in recruitment and activation of a MAPK module composed of Ste11, Ste7 and the MAPKs Fus3 and Kss1 (Alvaro and Thorner, 2016)). Fus3 then phosphorylates and stimulates the transcription factor Ste12 (Elion et al., 1993), which induces a transcriptional program required for efficient mating. Membrane-localized Far1 mediates polarized growth by recruiting the guanine nucleotide exchange factor Cdc24, which stimulates Cdc42 to induce formation of a mating projection (shmoo) (Butty et al., 1998). Cdc42 also activates the PAK-like kinase Ste20, which reinforces activation of the Fus3 MAPK pathway by phosphorylating Ste11 (Pryciak and Huntress, 1998).

Several feedback loops have been identified in the pheromone signaling pathway that improve transmission of information and that help switch off the pathway. An example of positive feedback is the increased expression of *FUS3* that occurs upon activation of Ste12 by Fus3 (Roberts et al., 2000). However, Fus3 also provides negative feedback to dampen the response and help switch off the mating response (Yu et al., 2008). This is physiologically relevant, because hyperactivation of the mating pathway, or an attempt to mate in absence of a partner, can lead to cell death (Severin and Hyman, 2002; Zhang et al., 2006), which can be caused by weakening of the cell wall during formation of the mating projection (Iida et al.,

1990; van Drogen et al., 2019). A major negative feedback mechanism consists of Fus3-mediated phosphorylation of Ste5, which attenuates signaling output (Choudhury et al., 2018; Repetto et al., 2018). Another example of Fus3-mediated negative feedback occurs through phosphorylation of Sst2 (Yu et al., 2008). Sst2 is a Regulator of G protein Signaling (RGS) and inhibits G-protein signaling by acting as a GTPase Activating Protein (GAP) for Gpa1 (Apanovitch et al., 1998), and it mediates desensitization of cells after pheromone treatment (Dohlman et al., 1995). Interestingly, Sst2 has also been shown to function as a noise suppressor (Dixit et al., 2014a). The dominant source of variation in the pheromone pathway is thought to be extrinsic noise (Colman-Lerner et al., 2005), and mutant cells either lacking *SST2* or expressing a mutant form of Gpa1 that is resistant to the GAP activity of Sst2 show increased levels of noise both in the transcription and in the morphogenesis branches of the pathway (Dixit et al., 2014a). Noise suppression is thought to be required for proper gradient detection and morphogenesis, and one potential physiological consequence of elevated noise in mutant cells is reduced mating efficiency (Dixit et al., 2014a).

Despite the fact that pheromone signaling has been studied intensively during the past decades, there are still several genes with poorly characterized functions in the pathway. One such gene is *KEL1*, which encodes a 131 kDa protein consisting of a KELCH propeller in the N-terminal region and three coiled-coil domains in the C-terminal region (Fig. 1B). Kel1 was first identified in a screen for genes whose overexpression relieved the mating defect caused by activated alleles of *PKC1* (Philips and Herskowitz, 1998). *kel1Δ* mutants are elongated and heterogeneous in shape and have a defect in cell fusion. Kel1 localizes to sites of polarized growth and forms a ternary complex with the cell fusion regulator Fus2 and activated Cdc42 during mating. Kel1 also interacts with formins to regulate the assembly of actin cables (Gould et al., 2014). These findings suggest that Kel1 may serve as a hub during the

pheromone response, but how and to which extent Kel1 controls the pheromone response remains unknown.

Here, we characterized the function of Kel1 in the pheromone response. We present data showing that Kel1 is regulated by phosphorylation, suppresses spontaneous activation of the pheromone pathway, has a major role in filtering noise in the pheromone pathway, and that it prevents pheromone-induced cell death.

Results

Kel1 is important for the pheromone response

During the course of our experiments, we serendipitously observed that approximately 35% of *kel1*Δ mutant cells died upon treatment with pheromone (Fig. 1C-E). Careful inspection of the data revealed that also a small but significant number of wild-type (WT) cells died after pheromone treatment (Fig. 1E), consistent with previous findings that mating is a potentially lethal affair (Severin and Hyman, 2002). The importance of Kel1 in preventing cell death was reflected in pheromone halo assays, where we observed a 30% cell-density reduction in the *kel1*Δ strain compared with the WT strain inside the halo, where the concentration of pheromone is highest (Fig. 1F, G). Although there was no significant change in the area of the halo, which is typically observed in mutants with defects in the mating pathway, we did notice a sharper interface of the halo (Fig. 1F, G), consistent with a role for Kel1 in the adaptive response to pheromone. Light microscopy revealed not only that *kel1*Δ mutants had significant morphological defects during vegetative growth, such as elongated buds and misshapen cells (Suppl. Fig. S1A, B), but more importantly, they were also 15 times more prone than WT cells to initiate the development of more than one shmoo during pheromone treatment (Fig. 1H). This indicates that *kel1*Δ mutants fail to commit to the original projection, resulting in abandonment of shmoos.

Together, these data indicate that Kel1 prevents pheromone-associated cell death.

Kel1 activity is regulated by phosphorylation

High-throughput experiments have detected at least 50 phosphorylated amino acids in Kel1, suggesting that Kel1 may be regulated by certain signaling pathways (Albuquerque et al., 2008; Bodenmiller et al., 2010; Gnad et al., 2009; Helbig et al., 2010; Holt et al., 2009; Li et al., 2007; Smolka et al., 2007). Indeed, λ-phosphatase treatment of immunoprecipitated

Kel1 resulted in increased mobility on SDS-PAGE, confirming that Kel1 exists as a phosphoprotein *in vivo* (Fig. 2A). It should be noted that bulk Kel1 phosphorylation did not appear to be altered much by pheromone treatment (Fig. 2A), even though it has previously been shown that phosphorylation of certain residues in Kel1 is increased after treatment with pheromone (Li et al., 2007). Likely, only a few phosphorylation sites in Kel1 respond to pheromone treatment, and their effect on the mobility of Kel1 on SDS-PAGE may be obscured by the other phosphorylation sites.

A substantial number of putative phosphorylation sites in Kel1 consists of [S/T-P] sites (Albuquerque et al., 2008; Bodenmiller et al., 2010; Gnad et al., 2009; Helbig et al., 2010; Holt et al., 2009; Li et al., 2007; Smolka et al., 2007), which are typically targeted by proline-directed kinases such as CDKs and MAPKs. One such kinase is the pheromone-activated MAPK Fus3, and several proline-directed phosphorylation sites in Kel1 have been detected specifically during pheromone treatment (Li et al., 2007). We hypothesized that proline-directed phosphorylation might regulate Kel1. Therefore, we first constructed two mutant alleles in which all [S/T-P] sites were substituted with either alanine or aspartate residues (*kel1-ala* and *kel1-asp*, respectively, see Methods for details). These alleles were fused to a C-terminal FLAG tag and integrated into the *KEL1* locus under control of the endogenous *KEL1* promoter. Phos-tag gel electrophoresis of immunoprecipitated proteins revealed that Kel1-ala migrated faster than wild-type Kel1, confirming that at least some of these [S/T-P] sites are phosphorylated *in vivo* (Fig. 2B). Although follow-up experiments are required to tease out exactly which specific [S/T-P] sites are regulated by pheromone, these data show that Kel1 is phosphorylated on one or several [S/T-P] sites *in vivo*.

Next, we analyzed the morphology of *kel1-ala* and *kel1-asp* mutant cells. We noticed that during vegetative growth the bud shape of WT cells was slightly oblong, whereas the

kel1-ala buds were almost perfectly spherical (Fig. 2C, D). *kel1-asp* buds were significantly more elongated than WT buds, although not as much as those of *kel1*Δ cells (Fig. 2C, D), and both *kel1-asp* and *kel1Δ* mutant cells frequently showed aberrant morphology (Fig. 2E). More importantly, upon pheromone treatment more than half of the *kel1-ala* mutant cells failed to form a shmoo (Fig. 2C, F), and those cells that did form a shmoo always generated a single, highly spherical shmoo (see below). In contrast, *kel1-asp* mutant cells readily formed shmoos and were more likely to form multiple shmoos after pheromone treatment than WT cells (Fig. 2F). Thus, the phenotype of *kel1-asp* cells resembles that of *kel1*Δ mutant cells, albeit more modest. Pheromone-associated cell death was also significantly higher in *kel1-asp* mutants, whereas in *kel1-ala* mutants it was significantly lower than in WT cells (Fig. 2G, H). This was reflected in the pheromone halo assay, which showed that the cell-growth interphase was sharper in the *kel1-asp* strain and more diffuse in the *kel1-ala* mutant compared to the WT strain (Fig. 2I, J). Finally, we analyzed the ability of the *kel1* mutants to mate with WT cells of the opposite mating type, which revealed that the mating capacity of *kel1*Δ and *kel1-ala* mutants was reduced significantly (Fig. 2K).

Taken together, these results indicate that phosphorylation of Kel1 is important for regulation of the mating process. Given that *kel1-ala* mutants have a phenotype opposite to that of phospho-mimicking *kel1-asp* mutants, and that the phenotype of *kel1-asp* cells generally resembles that of *kel1*Δ cells (although milder), we conclude that (i) hypophosphorylated Kel1 suppresses the pheromone response, and (ii) phosphorylation of certain [S/T-P] sites relieves the inhibitory effect of Kel1 on the pheromone response.

Kel1 acts downstream of Sst2 during the mating response

To identify pathways associated with phosphorylation of Kel1 we performed a genome-wide synthetic genetic array (SGA) screen (Baryshnikova et al., 2010; Tong et al.,

2001b). Since *kel1-asp* mutants have a loss-of-function phenotype that generally resembles that of the *kel1*Δ strain, but weaker, we decided to use only the *kel1*Δ and *kel1-ala* strains as query mutants. These mutants were crossed into the library of non-essential knock-out genes as well as the Decreased Abundance by mRNA Perturbation (DAmP) library (Breslow et al., 2008; Giaever et al., 2002). For all genetic interactions we calculated the genetic interaction score (see Methods). We focused on a subset of genes that showed differential genetic interactions with the *kel1*Δ and *kel1-ala* mutations, using a strict cut-off in which the difference between *kel1-ala* and *kel1*Δ scores deviated more than three standard deviations from the mean (Fig. 3A, Suppl. Fig. S1C, and Suppl. Table S1). To find patterns in this gene list, we studied the reported phenotypes for these genes using information gathered from the *Saccharomyces* Genome Database. The most highly overrepresented phenotype was *"Resistance to enzymatic treatment"* (Fig. 3B). Mutations in genes associated with this phenotype often lead to cell wall defects, resulting in increased sensitivity to cell wall-lytic enzymes. This is consistent with our finding that *kel1*Δ mutants frequently undergo cell death during pheromone-induced cell wall remodeling. The second most overrepresented phenotype was *"Mating response"*. This is likely an underestimate, because many pheromone-associated genes are not easily identified in SGA screens due to the fact that mutations in this pathway lead to severe mating defects, and efficient mating is essential for the genome-wide crosses that form the basis of SGA screening.

We were intrigued by one mating response-associated gene in particular, i.e. *SST2*, which encodes a Regulator of G protein Signaling (RGS) that suppresses the pheromone response (Dohlman et al., 1996). Loss of *SST2* substantially reduced the fitness of *kel1*Δ mutants, but did not appear to have a strong effect on the fitness of *kel1-ala* mutants (Fig. 3A). Interestingly, even in absence of pheromone approximately 8% of the cells in *sst2*Δ *kel1*Δ cultures were dead (Fig. 3C, D), consistent with the reduced growth of this mutant in

the SGA screen. Pheromone treatment strongly increased cell death of *kel1*Δ mutants, and although cell death in *sst2*Δ cultures was similar to WT (Fig. 3D), it was significantly higher in *sst2*Δ *kel1*Δ double mutants than in either single mutant (Fig. 3C, D).

We next studied the cellular morphology of the mutants in presence and absence of pheromone. 15% of vegetatively growing *sst2*Δ cells showed aberrant morphology, and the buds of *sst2*Δ mutants were generally more elongated than those of WT cells, but to a lesser extent than *kel1*Δ mutants (Fig. 3E-G). Pheromone treatment resulted in a small but significant increase in the number of *sst2*Δ cells with multiple projections (Fig. 3H). The morphology of cells and buds of the *sst2*Δ *kel1*Δ double mutant resembled that of the *kel1*Δ single mutant (Fig. 3F, G), and pheromone treatment of *sst2*Δ *kel1*Δ double mutants did not further increase the number of cells with multiple projections compared with the *kel1*Δ single mutant (Fig. 3E, H). However, the *kel1-ala* mutation completely suppressed the morphological defects and inhibited shmoo formation of *sst2*Δ mutants (Fig. 3E-H).

Taken together, these data show that Kel1 and Sst2 regulate cell morphogenesis both during vegetative growth and in the presence of pheromone, with Kel1 having a dominant role, and that Kel1 functions downstream of Sst2 in this process.

Kel1 physically interacts with pheromone pathway components and may be phosphorylated by Fus3 and Kss1

We wished to better understand how Kel1 is regulated during the pheromone response. We immunopurified Kel1 from untreated and pheromone-treated cells and identified interaction partners using mass-spectrometry (Tables S2 and S3). We identified a large number of proteins previously known to physically interact with Kel1, thus validating the approach (Suppl. Fig. S1D). We looked for proteins that differentially interacted with Kel1 depending on pheromone treatment, and observed a significant enrichment of proteins with

functions in the mating response (Fig. 4A), including Far1, Sst2, Fig1, the pheromone receptor Ste2 and the MAPK Fus3. We validated the pheromone-induced interaction between Kel1 and Ste2 and Fus3 in co-immunoprecipitation experiments (Fig. 4B). The interaction with the proline-directed kinase Fus3 piqued our interest, since Kel1 is phosphorylated on [S/T-P] sites in vivo. We hypothesized that Fus3, and perhaps the related kinase Kss1, could be required for phosphorylation of Kel1. We evaluated phosphorylation of Kel1 in *fus3*Δ and *kss1*Δ single mutants and in a *fus3*Δ *kss1*Δ double mutant using PhosTag gels (Kinoshita et al., 2006). Interestingly, the mobility of Kel1 was increased in the *fus3*Δ and *kss1*Δ single mutants and in the *fus3*Δ *kss1*Δ double mutant (Fig. 4C). A substantial amount of Kel1 remained phosphorylated, which is likely due to phosphorylation of Kel1 by other kinases on non-[S/T-P] sites. Although we presently cannot exclude the possibility that Fus3 and Kss1 have an indirect effect on Kel1 phosphorylation, the simplest interpretation of these results is that Fus3 and Kss1 phosphorylate Kel1 *in vivo*.

Kel1 prevents spontaneous recruitment of Ste5 and Far1 to inhibit formation of mating projections in absence of pheromone

Vegetatively growing *kel1Δ* mutant cells often form elongated structures that resemble shmoos. To determine whether these structures are indeed spontaneous shmoos we monitored membrane localization of Ste5 and Far1, which are markers for formation of mating projections (Nern and Arkowitz, 1999). Strikingly, even in absence of pheromone, we observed that NeonGreen (mNG)-tagged Ste5 and Far1 were recruited to patches at the cell cortex both in *kel1Δ* mutants and in *kel1-asp* mutant cells (Fig. 5A, B). Such spontaneous membrane recruitment of Ste5 and Far1 was not observed in WT cells or in *kel1-ala* mutants. Furthermore, whereas pheromone treatment resulted in localization of Ste5-mNG and Far-mNG at the cortex of WT cells, recruitment of these proteins was undetectable in the *kel1-ala*

mutant (Fig. 5A-C). These findings show that the polarized structures that are observed in vegetatively growing *kel1*Δ and *kel1-asp* mutants are indeed spontaneous shmoos, and suggest that Kel1 suppresses spontaneous signaling through the pheromone pathway. Therefore, we analyzed the mRNA levels of two genes known to be upregulated by the pheromone pathway, i.e. *FUS3* and *STE2* (Oehlen et al., 1996). Although there was no significant difference in *FUS3* and *STE2* mRNA levels between populations of WT cells and any of the *kel1* mutants after pheromone treatment, *kel1*Δ mutant populations showed a significant increase in mRNA levels in absence of pheromone (Fig. 5D), confirming that Kel1 suppresses spontaneous activity of the pheromone pathway.

If Kel1 indeed inhibits spontaneous signaling through the pheromone pathway by preventing the accumulation of Ste5 at the cell cortex, then deletion of *STE5* should reverse the phenotype of *kel1*Δ and *kel-asp* mutants. We found that the buds of vegetatively growing *ste5*Δ mutants were significantly more spherical than those of WT cells (Fig. 5E, F). More importantly, deletion of *STE5* also modestly but significantly reduced the bud phenotype of *kel1*Δ and *kel1-asp* mutant cells (Fig. 5E, F), and strongly reduced the fraction of cells with aberrant cell morphology (Fig. 5G). Finally, deletion of *STE5* almost completely rescued pheromone treatment-induced lethality in *kel1*Δ and *kel1-asp* mutants (Fig. 5H, I). These data show that Kel1 suppresses spontaneous activation of the pheromone pathway by preventing aberrant recruitment of Ste5 to the cell cortex.

Hypophosphorylated Kel1 cooperates with Sst2 to prevent spontaneous pheromone signaling and to dampen the pheromone response

Spontaneous activation of the pheromone pathway has been observed previously and was found to originate downstream of the receptor at the level of the G protein (Siekhaus and Drubin, 2003), which we confirmed (Suppl. Fig. S1E). Mechanisms have evolved that

suppress spontaneous signaling; for instance, RGS proteins like Sst2 inhibit unscheduled G protein signaling (Siekhaus and Drubin, 2003). Given our findings that Kel1 acts downstream of Sst2 but at/upstream of Ste5, and that the *kel1-ala* mutant suppresses the morphological defects observed in *sst2*Δ mutant cells, we hypothesized that Kel1 might cooperate with Sst2 to inhibit spontaneous signaling. We made use of a dual reporter system based on expression of GFP under control of the pheromone pathway-sensitive *FUS1* promoter and mCherry under control of the pheromone pathway-independent *ADH1* promoter; the ratio of GFP/mCherry is a measure of signaling pathway activity at single-cell resolution (Dixit et al., 2014a). Interestingly, single-cell microscopy revealed that in absence of pheromone the GFP/mCherry ratio was significantly higher in *kel1*Δ mutants than in WT cells ("0 min" in Fig. 6A; timecourse in Fig. 6B; quantification in Fig. 6C). In contrast, the signal level in *kel1-ala* mutants was significantly lower than in WT cells (Fig. 6A-C), confirming our finding that hyposphosphorylated Kel1 serves as a major signal suppressor in absence of stimulus. We then analyzed the relative contributions of Sst2 and Kel1 in suppressing spontaneous activity of the signaling pathway. As expected, in absence of pheromone the basal level of the signal was higher in the *sst2*Δ mutant than in the WT strain, and was similar to that of *kel1*Δ mutants (Fig. 6A-C). However, *sst2*Δ *kel1*Δ double mutants had significantly higher basal signaling levels than either single mutant, whereas the *kel1-ala* mutation suppressed spontaneous pathway activity in the *sst2*Δ mutant (Fig. 6A-C).

Next, we treated the different strains with pheromone and monitored cellular responses using single-cell time-lapse microscopy. Compared to the WT strain, the signal amplitude was higher in the majority of *kel1*Δ mutants and lower in *kel1-ala* mutants (Fig. 6A, D and Suppl. Fig. S3A). Quantification of the signal after 180 min of pheromone treatment supported these findings (Fig. 6E). As expected, pheromone treatment resulted in a generally higher amplitude in *sst2*Δ cells than in WT cells (Fig. 6A-C), but strikingly, expression of *kel1-ala* in the *sst2*Δ

background reduced the output of the pheromone signaling pathway to a level comparable to that of WT cells (Fig. 6A,D,E). These data are consistent with an inhibitory role of hypophosphorylated Kel1 downstream of Sst2.

Kel1 suppresses noise in the pheromone signaling pathway

We noticed that there existed considerable cell-to-cell variability in the pheromone response in the population of *kel1Δ* mutants, which suggests that Kel1 may suppress noise in the mating pathway. To investigate this further, we measured the overall signaling noise as the coefficient of variation (CV) of the median population response before and after pheromone treatment. The dispersion in WT signaling was between 40-50% both before and after pheromone treatment, but increased slightly in the dynamic range of the pheromone response as previously reported (Fig. 7A, B and Suppl. Fig. S3B)(Dixit et al., 2014b). Interestingly, the signal dispersion in untreated cell populations was higher in *kel1*Δ mutants than in WT cells, but strongly reduced in *kel1-ala* mutants (Fig. 7A, B and Suppl. Fig. S3B). As expected, signal dispersion was also slightly increased in the *sst2*Δ mutant, although less so than in the *kel1Δ* strain, while expression of *kel1-ala* reduced the variability of the *sst2*Δ mutant to that of the WT strain. In contrast, after 180 minutes of pheromone treatment we could no longer observe the increase in overall noise that we detected in populations of *kel1Δ* and *sst2*Δ mutants in absence of pheromone (Fig. 7B). This is likely a consequence of the elevated signaling and increases in average GFP expression in these mutants, which causes an expected decrease in CV for overdispersed distributions (Fig. 6)(Eling et al., 2019). Interestingly, the CV increased in the *kel1-ala* mutant in response to pheromone (Fig. 7A, B and Suppl. Fig. S3B). The increased signaling variability in the *kel1Δ* mutant and the suppressive effect of *kel1-ala* on the *sst2*Δ phenotype in the absence of pheromone caused us to speculate whether Kel1 serves to suppress intrinsic signaling noise and spontaneous

activation of the signaling pathway, while maintaining high signaling fidelity in response to pheromone. To investigate this, we used regression to estimate the intrinsic noise from non-reducible residual fluctuations over modeled signaling trajectories for individual cells (Hilfinger and Paulsson, 2011). By using a linear model in the linear range of the pheromone signaling response, we observed a substantial increase in variation over the predicted signaling trajectories in the *kel1Δ* mutant and the *kel1Δ sst2Δ* double mutant compared to the WT strain (Fig. 7C, D). The *sst2Δ* mutation alone caused a more moderate increase in residual variation, which was completely abolished by expression of the *kel1-ala* allele (Fig. 7C, D). Taken together, these results show that Kel1 suppresses noise and limits spontaneous signal transmission in the absence of pheromone.

Discussion

High levels of noise in signaling pathways can result in a substantial fitness cost, and therefore filtering mechanisms have evolved to suppress noise. Here, we identify Kel1 as a major noise suppressor in the pheromone pathway. Importantly, Kel1 is regulated by phosphorylation, particularly on [S/T-P] sites, and it is the hypophoshorylated form of Kel1 that mediates noise suppression, inhibits spontaneous activation of the pathway, and that prevents cell death during pheromone treatment. Although additional experiments are required to firmly establish the kinase(s) that phosphorylate Kel1, our data are consistent with a model in which the negative effects of Kel1 on the pheromone pathway are relieved by Fus3 Kss1-mediated phosphorylation and thereby inhibition of Kel1.

What could be the physiological relevance of Kel1 during mating? In absence of pheromone, or under suboptimal mating conditions where mates are only transiently available, such as in dynamic aqueous environments, hypophoshorylated Kel1 may prevent activation of the response to avoid unsuccessful mating attempts. Inappropriate activation of the pathway is associated with a fitness cost (Banderas et al., 2016), and we found that cells lacking Kel1 have a mating defect and are prone to cell death upon exposure to pheromone. Our working model is shown in Suppl. Figure S2. In absence of pheromone, hypophosphorylated Kel1 prevents recruitment of Ste5 and Far1 to the cell membrane (Suppl. Fig. S2A). When pheromone is detected, Kel1 becomes phosphorylated in a manner dependent on Fus3/Kss1, potentially setting up a double-negative feedback loop to boost the pheromone response (Suppl. Fig. S2B); such double-negative feedback loops can act as bistable switches, resulting in rapid all-or-none changes in cellular states (Ferrell, 2002) and previous findings indicate Ste5-dependent switch-like behavior of the mating pathway (Malleshaiah et al., 2010; Paliwal et al., 2007); it will be interesting to test if and how Kel1 affects switch-like decision-making in the pheromone pathway. Regardless of the outcome of

such experiments, Ste5 is aberrantly recruited to the membrane in a fraction of *kel1Δ* mutant cells, resulting in activation of the mating transcriptional program and spontaneous formation of mating projections (Suppl. Fig. S2C), and pheromone treatment of these cells results in excessive activation of the pathway and increases the risk of cell death (Suppl. Fig. S2D). Expression of non-phosphorylatable Kel1-ala blunts pheromone-induced recruitment of Ste5 (Suppl. Fig. S2E), suppresses noise in the pathway and reduces pheromone-induced cell death, limits formation of mating projections and results in low mating efficiency.

The *kel1-asp* mutant partially phenocopied the *kel1Δ* mutation, which is consistent with the idea that, at least in terms of the pheromone response, hypophosphorylated Kel1 suppresses the pathway, whereas phosphorylation of Kel1 results in its inactivation. It should be mentioned that the effects of the *kel1-asp* mutant were generally milder than the *kel1Δ* mutation, which could at least partially be due to the fact that phosphomimicking residues often do not fully replicate the effect of phosphorylation (Paleologou et al., 2008). Some of the other limitations of our study that remain to be addressed are to determine the exact phosphorylation sites in Kel1 that respond to pheromone, identify the phosphatase that targets Kel1, and unravel the molecular mechanism by which Kel1 controls activity of the mating pathway. We presently also do not know how phosphorylation regulates the function of Kel1 at the molecular level. Kel1 consists of a Kelch propeller and coiled coil domains, which are known to mediate multimerization and protein-protein interactions. Given that Kel1 can physically interact with Ste2, Sst2, Far1, Ste5, Fus3, we speculate that Kel1 may form a phospho-dependent platform that integrates signals to regulate the pheromone pathway. Future studies will focus on unraveling the molecular mechanism by which Kel1 regulates membrane recruitment of Ste5 and Far1.

In addition to [S/T-P] sites, Kel1 appears to be phosphorylated on many other sites, suggesting that several other signaling pathways may converge onto Kel1. Interestingly, it

was recently shown that in response to mechanical stress Pkc1 prevents lysis of pheromone-treated cells by phosphorylating Ste5, resulting in dispersal of Ste5 from the site of polarized growth (van Drogen et al., 2019). We found that Kel1 also suppresses lysis during pheromone treatment and that it regulates Ste5 localization. Moreover, Kel1 was first identified in an overexpression screen for genes that overcome the fusion defect of cells expressing activated Pkc1 (Philips and Herskowitz, 1998). It will be interesting to investigate the relationship between Pkc1, Kel1 and Ste5 at the molecular level.

Computer simulations and experimental studies have revealed mechanisms that provide robustness to the mating response (Chen et al., 2016; Howell et al., 2012), which is defined here as the persistence of a system's behavior under conditions of uncertainty. Robustness is critical for efficient yeast mating and one way cells improve robustness is by reducing the sensitivity to pheromone, which is in part mediated by Sst2 (Chen et al., 2016). We found that the transcriptional response to pheromone in individual *kel1Δ* mutant cells fluctuated considerably over time, whereas *kel1-ala* mutants showed less fluctuations compared to WT cells. This suggests that, whereas phosphorylation of Kel1 promotes activity of the pathway, hypophosphorylated Kel1 may provide robustness to the system. The phenotype of the *kel1Δ* mutant and the *kel1-ala* mutant masked the increase in signaling noise in *sst2Δ* mutants, indicating that proper control of Ste5 may be the dominant limiting factor for signal transmission fidelity and amplitude. We speculate that the balance between phosphorylated and a hypophosphorylated Kel1 is important for fine-tuning the output of the pathway by controlling Ste5. Clearly, more studies are needed to more fully understand how Kel1 regulates pheromone signaling.

In conclusion, we have shown that Kel1 is an important regulator of the mating pathway with a major function in noise suppression.

Methods

Yeast strains and growth conditions

S. cerevisiae strains were grown in at 30°C until mid-log phase in standard yeast extract peptone dextrose (YPD) medium or in synthetic medium supplemented with relevant amino acids. Strains were derived directly from the S288c strains BY4741 (Brachmann et al., 1998) and RDKY3032 (Flores-Rozas and Kolodner, 1998) using either standard gene-replacement methods or intercrossing. See Suppl. Table S3 for strains.

To construct *kel1-ala* and *kel1-asp* mutants, *KEL1* was fist replaced with the *URA3* gene. Next, the *URA3* on the strain *kel1::URA3* was replaced by *kel1-ala* and *kel1-asp* alleles, which were PCR-amplified from plasmids containing in vitro synthesized *kel1* alleles in which the S/T-P sites were replaced with either alanine or aspartate residues, respectively. In some cases where two or three serine/threonine residues preceded a proline, all were substituted. Note that *kel1-asp* differs slightly from *kel1-ala* in terms of mutated sites (additional substitution of T65 and S688). Alanine substitutions in Kel1-ala: T18, S34, T35, T47, S66, S67, S121, T178, T293, T465, T467, T477, T480, S503, T549, T559, T604, S613, T626, S689, S748. Aspartate substitutions in Kel1-asp: T18, S34, T35, T47, T65, S66, S67, S121, T178, T293, T465, T467, T477, T480, S503, T549, T559, T604, S613, T626, S688, S689, S748.

Plasmids

For a list of plasmids see Suppl. Table S4. The pFA6-mNG plasmid was generated by replacing the eGFP coding sequence from pYM-28 (Janke et al., 2004) by codon-optimized monomeric NeonGreen (mNG) DNA sequence (Shaner et al., 2013) synthesized by GeneScript. mNG sequence was amplified using primers NG-FW and NG-RV (For primers

see respectively Suppl. Table S5), which also include *HindIII* and *BamHI* sites for the tag replacement.

Pheromone treatment

Cells were treated with 15mg/L of alpha actor (custom synthesized by GenScript) for 2 hrs unless otherwise indicated.

Mating efficiency assay

To evaluate the matting efficiency 1ml of mid-log-phase MATa and MATα cells carrying complementary markers were mixed an incubated at 30°C in absence of agitation for 4 hours. 100µl of five consecutive serial dilutions (1:10) of the crosses were plated on YPD plates and diploid selective media (YPD supplemented with G418 200µg/ml (Sigma) and nourseothricin 100µg/ml (WERNER)). After 2 days of incubation at 30°C the colonies of the plates were counted using the Colony Counter mobile application (Promega). See Suppl. Table S3 for strains.

FITC staining

Cells were harvested, washed with PBS and stained for 10 min in the dark with 1mg/ml FITC (Sigma-Aldrich) in carbonate buffer (0.1M, pH 9.5). Cells were washed 3 times with PBS and visualized with the microscope.

Flow cytometry

GFP and RFP-expressing cells were harvested and fixed with 4% paraformaldehyde for 15 min at room temperature. Paraformaldehyde was quenched with Glycine 0.5M for 15 min at room temperature. Cells were washed 2 times with PBS, resuspended in PBS and sonicated

for 10 seconds at 30% amplitude. Flow cytometry was performed using an LSR II Flow Cytometer (BD Biosciences). Data analysis and plotting was performed in R.

Mass spectrometry

Cells untreated or treated with α-factor for 2 hrs. were collected, washed with cold PBS and lysed in lysis buffer (100mM Tris-HCl pH8, 150mM NaCl, 1mM EDTA, 1% Triton X-100, 10% Glycerol, 2mM DTT, protease and phosphatase inhibitor cocktails). After centrifugation, supernatants were immunoprecipitated by mixing 800 µg of cell extract with 20 µl of anti-Myc-Tag magnetic bead (Cell Signaling). After 2 hrs. incubation at 4°C, beads were washed once with wash buffer A (100mM Tris-HCl pH8, 150mM NaCl, 1mM EDTA, 5% Glycerol, 2mM DTT, protease and phosphatase inhibitor cocktails), twice with wash buffer B (100mM Tris-HCl pH8, 150mM NaCl, 1mM EDTA, 2mM DTT, protease and phosphatase inhibitor cocktails) and twice with PBS. MS samples were processed at the Proteomics Core Facility at Oslo University Hospital. All MS data were deposited to the ProteomeXchange Consortium via PRIDE repository with accession number PXD020833.

Cell lysis, immunoprecipitation, λ phosphatase treatment and Western blotting

Immunoprecipitation and Western blotting were performed as previously described (Chymkowitch et al., 2012; Chymkowitch et al., 2017; Herrera et al., 2018). For coimmunoprecipitations, cells were washed with cold PBS, resuspended in lysis buffer (100mM Tris-HCl pH8, 150mM NaCl, 1mM EDTA, 1% Triton X-100, 10% Glycerol, 2mM DTT, protease and phosphatase inhibitor cocktails) and lysed by vortexing with glass beads followed by centrifugation to remove cell debris. Equal amounts of proteins were used for immunoprecipitation using magnetic beads conjugated covalently to relevant antibodies. After

extensive washing with lysis buffer, coimmunoprecipitated proteins were resolved by SDS-PAGE and analyzed by Western-blotting with the indicated antibodies.

For λ phosphatase treatments, cells were harvested and lysed as described above, magnetic beads were washed 2 times with lysis buffer without phosphatase inhibitors. Samples were treated with 800 units of λ-phosphatase (NEB) for 30 min after which the enzyme was heat-inactivated (5 min at 95ºC) and the proteins resolved by SDS-PAGE and analyzed by Western-blotting.

Phos-tag gel electrophoresis

Phos-tag gel electrophoresis was performed as previously described (Herrera et al., 2018). Briefly, cells were harvested and washed with ice-cold 20% TCA (Sigma-Aldrich) and resuspended in 20% TCA. Cells were lysed by vortexing with glass beads followed by centrifugation (10 min. at 13.000 rpm). Precipitated proteins were washed with ethanol 70%. Equal amounts of sample were loaded onto 4.5% acrylamide (*BioRad*) 20μM Phos-tag (Supersep, Wako chemicals) gels, followed by electrophoresis for 6 hours at 150 V. Gels were washed three times for 10 min with transfer buffer containing 5 mM EDTA and three times for 10 min with transfer buffer without containing EDTA. The gel was transferred to a membrane and protein phosphorylation was analyzed by Western blotting as described above. Protein densitometric quantifications were performed using FIJI software (Schindelin et al., 2012) and analyzed using R.

Microscopy

DIC images (Fig. 1C, H and 2C) were acquired on a Leica DM600B microscope using a 63X/1.40NA immersion objective. The microscope was connected to a Hamamatsu C9100-14 camera controlled by Leica Application Suite software.

FITC staining (Fig. 1D, 2G, 3C and 5H) Far1-mNG (Fig. 5B) and brightfield images (Fig. 3E and 5E) were acquired using a Zeiss AXIO Scope.A1 microscope containing a 63X/1.40NA immersion objective and a Leica DFC camera. The microscope was controlled by Micro-Manager software (Edelstein et al., 2010). Ste5-mNG images (Fig. 5A) were obtained using a Zeiss AXIO Observer.Z1 microscope containing a 63X/1.40NA immersion objective. The microscope was equipped with a Hamamatsu ORCA-Flash4.0 camera and temperature control and it was controlled by Micro-Manager software.

Synthetic genetic array (SGA)

The SGA query strain Y8205 (*can1::STE2pr-Sp_his5 lyp1::STE3pr-LEU2 his3Δ1 leu2Δ0 ura3Δ0*; kind gift from C. Boone, University of Toronto, Canada) either harboring the *kel1Δ* or the *kel1-ala* mutation was crossed with a collection of deletions of non-essential genes (YKO) and with a collection of mutants with reduced mRNA levels of essential yeast genes (DAmP) according to (Tong et al., 2001a). Briefly, mutations of interest were linked to natMX selectable marker, while mutations in the collections to kanMX. After mating and sporulation, the spores were transferred to medium which enables growth of MATa meiotic progeny. In a last step, double mutants were obtained after selection on medium containing kanamycin and nourseothricin. Each cross was done in quadruplicate on 1536-format plates. All double mutants were grown at 30°C and 37°C and imaged after 2 days. Image analysis and scoring were done with SGAtools (Wagih et al., 2013).

The phenotype enrichment score (Fig. 3B) was computed in R using the bc3net library (de Matos Simoes et al., 2012) and it was calculated over genes annotated with phenotypes in invasive growth, response to pheromone, pheromone sensitivity, mating projection morphology, cell shape, endomembrane system morphology, cell wall morphology and

cytoskeleton morphology. All annotations were downloaded from the Yeast Phenotype Ontology database (https://www.yeastgenome.org/ontology/phenotype/ypo).

RT-qPCR

RT-qPCR experiments were performed as previously described (Chymkowitch et al., 2012) (For primers see respectively Suppl. Table S5).

Author contributions

Designed research: NG and JME. Performed research: NG, PC, SMO, JE. Analyzed data: NG, JME, ANA, PC, SMO, JE. Wrote the paper: NG, ANA, JME.

Acknowledgments

This work was supported by grants from the Norwegian Cancer Society (project numbers 182524 and 208012), the Norwegian Health Authority South-East (2018012, 2017072) and the Norwegian Research Council (267454). This work was partly supported by the Research Council of Norway through its Centres of Excellence funding scheme, project number 262652.

Figure Legends

Figure 1. Kel1 prevents formation of multiple shmoos and suppresses cell death in the presence of pheromone. ***A,*** Overview of the pheromone response pathway. ***B***, Schematic representation of the secondary structure of Kel1. The 20 putative S/T[P] phosphorylation sites are indicated with red arrowheads. ***C***, *kel1*Δ mutant cells have morphological defects. DIC microscopic images of representative WT and *kel1*Δ cells in absence or presence of pheromone (15 mg/l) for 2 hrs. A substantial number of *kel1*Δ cells are elongated in absence of pheromone (arrow) and often die in presence of pheromone (asterisk). ***D***, Kel1 prevents cell death in presence of pheromone. Fluorescence microscope images of WT and *kel1*Δ cells incubated in absence or presence of pheromone (15 mg/l) for 2 hrs. Cells were stained with FITC (0.01 mg/ml) for 5 min to visualize cell death. ***E***, Percentages of WT and *kel1*Δ dead cells in absence or presence of pheromone (15 mg/l) for 2 hours. The bars represent the mean from three independent experiments and the error bars represent the bootstrapped-standard deviations (see Methods). Statistical significance was calculated using two-proportions z-tests, * $0.01<p<0.05$; *** $p<0.001$. ***F***, Pheromone sensitivity assay. Equal numbers of cells of the indicated strains were plated on YPD plates in the form of a top layer of agar. A sterile filter was placed on this top layer, 15 μg of alpha factor was pipetted onto the filter, and the plates were incubated at 30ºC until halos appeared. ***G***, Densitometric quantification of relative cell growth across the plates shown in (F). Statistical significance of the density at the region closer to the disc was calculated using t-test, standard deviation $p<0.001$. ***H***, Kel1 prevents the formation of multiple shmoos during pheromone response. Quantification of the number of shmoos per cell in cultures of WT and *kel1*Δ strains that had been treated with pheromone (15 mg/l) for 2 hrs. The bars represent the mean from three independent experiments and the error bars represent the bootstrapped-standard deviations. Statistical significance was calculated using two-proportions z-tests, *** $p<0.001$.

Figure 2. Kel1 is regulated by phosphorylation. ***A***, Kel1 exists as a phosphoprotein *in vivo*. Log-phase cultures were either left untreated or were treated with pheromone (15 mg/l) for 2 hrs, after which Kel1 was purified and treated with λ phosphatase as described in Methods. ***B***, Kel1-ala is hypophosphorylated. Kel1 and Kel1-ala were purified from log phase cultures and analyzed by Phos-tag SDS-PAGE. The lower panel shows the normalized densitometric quantification of the blot (see Methods). ***C***, Cell morphology is controlled by Kel1 phosphorylation. DIC microscopic images of representative WT, *kel1-ala* and *kel1-asp* cells in absence or presence of pheromone (15 mg/l) for 2 hrs. ***D,*** Quantification of bud ellipticity of the experiment shown in (C). Ellipticity was calculated as described in the Methods section. The mean and standard deviations for each strain are shown as red bars. Statistical significance was calculated using t-test, *** $p<0.001$. ***E,*** Quantification of cells with aberrant morphology in absence of pheromone (Figs. 1C and 2C). The bars represent the mean from three independent experiments and the error bars represent the bootstrapped-standard deviation. Statistical significance was calculated using two-proportions z-tests, *** $p<0.001$. ***F,*** Efficient shmoo formation requires Kel1 phosphorylation. Quantification of the number of shmoos per cell was performed as described in Fig. 1H, *** $p<0.001$. ***G,*** Increased death of *kel1-asp* mutants after treatment with pheromone. FITC staining to visualize cell death was performed as described in Fig. 1D. ***H,*** Quantification of cell death. Analysis was performed as described in Fig. 1E, * $0.01<p<0.05$. ***I,*** Pheromone filter assay. The experiment was performed as described in Fig. 1F with the indicated strains. ***J,*** Densitometric quantification of the experiment shown in (I). ***K,*** *kel1* mutants have mating defects. Mating efficiency assay was performed as described in Methods. The bars represents the mean from 3 independent experiments and error bars represent bootstrapped-standard deviation, *** $p<0.001$.

Figure 3. *KEL1* acts downstream of Sst2 in the pheromone response. *A,* Results of the SGA screen. Each dot represents a gene, while the coordinates represent genetic scores observed with the *kel1*Δ versus the *kel1-ala* strain. Colored dots represent genes with reported phenotypes in mating and/or resistance to Zymolyase 20T that show differential genetic scores in the *kel1* mutants. ***B,*** Gene ontology enrichment analysis of the genes showing differential genetic scores with *kel1*Δ and *kel1-ala*. Calculation of the enrichment was performed as described in Methods. ***C,*** Loss of *SST2* enhances the toxicity of pheromone in *kel1Δ* mutants. The experiment was performed as described in Figure 1D. ***D,*** Quantification of cell death. Analysis was performed as described in Figure 1E, *** $p<0.001$. ***E,*** *kel1-ala* suppresses the morphological defects of the *sst2*Δ mutant. Microscopic images of the indicated strains in absence or presence of pheromone (15 mg/l) for 2 hrs. Asterisk: Dead cells. ***F,*** Quantification of bud ellipticity of untreated cells in the experiment shown in (E). The analysis was performed as described in Figure 2D. Statistical significance was calculated using Tukey's range test, *** $p<0.001$. ***G,*** Quantification of cells with aberrant morphology in untreated cells (E) was performed as in Figure 2E, *** $p<0.001$. ***H,*** Expression of *kel1-ala* inhibits shmoo formation of *sst2*Δ mutant cells. Quantification of the number of shmoos per cell was performed as described in Figure 1H, * $0.01<p<0.05$; *** $p<0.001$.

Figure 4. Kel1 binds multiple components of the mating response pathway in response to pheromone. *A,* Volcano plot of IP-MS experiments using Myc-tagged Kel1 in absence or presence of pheromone (15 mg/l) for 2 hrs. Enrichment of interaction partners was determined by quantitative MS. Binding partners enriched more than 1.6 times after treatment with pheromone (p-value<0.013) are shown in red. ***B,*** Pheromone-induced physical interactions between Kel1-Ste2 and Kel1-Fus3. Myc-tagged Kel1 was immunoprecipitated from untreated or pheromone-treated (15 mg/l for 2 hrs) cells expressing Ste2-GFP, after which cell lysates

were analyzed by Western blotting using GFP- and Fus3-specific antibodies. ***C,*** Efficient phosphorylation of Kel1 requires Fus3 and Kss1. Analysis of Kel1 phosphorylation levels in the indicated strains was performed as described in Figure 2B.

Figure 5. Kel1 functions upstream of Ste5 to prevent spontaneous formation of shmoos. ***A,*** Kel1 prevents ectopic recruitment of Ste5 in absence of pheromone. Ste5 was tagged with mNeonGreen (Ste5-mNG) and visualized in living cells by fluorescence microscopy in absence or presence of pheromone (15 mg/l) for 2 hrs. Arrows indicate cortex-localized Ste5. ***B,*** Cortical recruitment of Far1-mNG was studied as in (A). ***C,*** Quantification of the overall intensity of Far1-mNG (B) in presence of pheromone. Bars represent the mean of the relative intensity and the error bars the standard deviation. Statistical significance was calculated using t-test, *** $p<0.001$. ***D,*** Kel1 prevents spontaneous expression of pheromone-induced mRNAs. *FUS3* and *STE2* mRNA levels were analyzed in WT and *kel1* mutants in absence and presence of pheromone (15 mg/l) for 2 hrs. mRNA levels were normalized to WT. Error bars represent standard deviation. Statistical significance was calculated using t-test, * $0.01<p<0.05$. ***E,*** Deletion of *STE5* partially rescues *kel1*Δ phenotypes. The indicated strains were incubated in absence or presence of pheromone (15 mg/l) for 2 hrs before imaging. ***F,*** Quantification of bud ellipticity of untreated cells in the experiment shown in (E). The mean and standard deviations for each strain are shown as red bars. Statistical significance was calculated using Tukey's range test, *** $p<0.001$. ***G,*** Quantification of cells with aberrant morphology in absence of pheromone of the experiment shown in (E). Analysis was performed as in Figure 2E, *** $p<0.001$. ***H,*** Deletion of *STE5* prevents cell death in the *kel1*Δ and *kel1-asp* mutants. Cell death was visualized by FITC staining as described in Figure 1D. WT image was taken from an independent experiment. ***I,*** Quantification of cell death of the

experiment shown in (H). Analysis was performed as described in Figure 1E, ** 0.001<p<0.01.

Figure 6. Kel1 dampens the pheromone signaling pathway. *A,* Representative micrographs of pheromone signaling time-courses. Populations of WT, *kel1*Δ, *kel1-ala*, *sst2*Δ, *sst2*Δ *kel1*Δ and *sst2*Δ *kel1-ala* strains carrying the reporter system *FUS1p*-GFP/*ADH1p*-mCherry were imaged by fluorescence microscopy at different timepoints in absence or presence of pheromone (15 mg/l). ***B,*** Pheromone signal trajectories in untreated cells. Cells were imaged every 10 min. After image alignment, cells were identified, labeled and tracked over time (60 min). For each individual cell the ratio of GFP/mCherrry intensities was measured and plotted (blue trajectories). The plot shows the cellular trajectories of one representative experiment. ***C,*** Median GFP/mCherry intensity in absence of pheromone. After 60 min in absence of pheromone, the median of the GFP/mCherry ratios was calculated for each strain and the values of 4 independent experiments (red dots) were plotted. Statistical significance was calculated using paired t-test, ** 0.001<p<0.01. ***D,*** Pheromone signal trajectories in presence of pheromone (15 mg/l for 180 min). The experiment was performed in similar conditions as in (B). ***E,*** Median GFP/mCherry intensity in presence of pheromone (15 mg/l for 180 min). The analysis was performed as described in (C). *** p<0.001; ** 0.001<p<0.01; * 0.01<p<0.05.

Figure 7. Kel1 prevents noise in the pheromone signaling pathway. *A,* Noise in the pheromone signaling pathway in absence of pheromone. Noise was computed as the ratio between the standard deviation and the median of the ratio of GFP and mCherry fluorescence intensities after 60 min in absence of pheromone from 4 independent experiments (red dots). Statistical significance was calculated using paired t-test. * 0.01<p<0.05 and ns, not

significant. ***B,*** Noise in the pheromone signaling pathway in presence of pheromone (15 mg/l for 180 min), calculated as in (A). ***C,*** Within-cell variations in the pheromone signaling pathway in presence of pheromone (15mg/l) of one representative experiment. Fluctuation trajectories of individual cells (blue lines) were calculated by computing the absolute error of the ratio of GFP and mCherry intensities from an averaged linear trajectory for each individual cell after addition of 15mg/l pheromone for 50-130 min. ***D,*** Median of the intrinsic residual error in the linear range (50-130 min) of the pheromone signaling pathway in cells treated with 15mg/l pheromone. The residual error was calculated as in (C). Statistical significance was calculated using paired t-test, *** $p<0.001$; ** $0.001<p<0.01$; * $0.01<p<0.05$. ns, not significant.

Supplemental Figure Legends

Figure S1. ***A,*** Kel1 suppresses elongated bud growth. WT cells and *kel1*Δ mutants were grown to log phase, imaged by light microscopy and bud ellipticity was calculated as indicated in the figure. ***B,*** Loss of *KEL1* results in morphological aberrancies. Quantification of morphology of cells imaged in S1A). ***C,*** Statistical cut-off of mutants analyzed in Figure 3A. ***D,*** Overview of known and novel physical interactions with Kel1 (see Figure 4A for description of the experiment). ***E,*** Noise in the pheromone signaling pathway is generated downstream of Ste2. The ratio of GFP/mCherry in the indicated mutants was determined by fluorescence microscopy.

Supplemental Figure S2. Model for regulation of the mating response by Kel1 phosphorylation. ***A,*** In absence of pheromone, hypophosphorylated Kel1 prevents spontaneous activation of the pheromone response by inhibiting recruitment of Ste5 and Far1 to the membrane, whereas Sst2 prevents spontaneous activation of the pathway by inhibiting Gpa1. ***B,*** Pheromone treatment results in dissociation of the beta-gamma subunit of the G protein, which induces membrane recruitment of Ste5 and Far1. This results in activation of the MAPKs Fus3 and Kss1, which phosphorylate and thereby inactivate Kel1, allowing for recruitment of additional Ste5 to induce robust activation of the pathway. ***C,*** In *kel1Δ* cells, Ste5 and Far localize spontaneously to the membrane even in absence of pheromone, resulting in increased transcription of pheromone response genes, shmoo formation and noise in the pathway. ***D,*** Pheromone treatment of cells lacking Kel1 results in hyperactivation of the mating pathway, high levels of noise, and cell death. ***E,*** Expression of non-phosphorylatable Kel1 inhibits membrane recruitment of Ste5 and Far1, thereby suppressing the pheromone pathway and strongly reducing noise.

References

Albuquerque, C.P., M.B. Smolka, S.H. Payne, V. Bafna, J. Eng, and H. Zhou. 2008. A multidimensional chromatography technology for in-depth phosphoproteome analysis. *Mol Cell Proteomics*. 7:1389-1396.

Alvaro, C.G., and J. Thorner. 2016. Heterotrimeric G Protein-coupled Receptor Signaling in Yeast Mating Pheromone Response. *J Biol Chem*. 291:7788-7795.

Apanovitch, D.M., T. Iiri, T. Karasawa, H.R. Bourne, and H.G. Dohlman. 1998. Second site suppressor mutations of a GTPase-deficient G-protein alpha-subunit - Selective inhibition of G beta gamma-mediated signaling. *Journal of Biological Chemistry*. 273:28597-28602.

Balazsi, G., A. van Oudenaarden, and J.J. Collins. 2011. Cellular decision making and biological noise: from microbes to mammals. *Cell*. 144:910-925.

Banderas, A., M. Koltai, A. Anders, and V. Sourjik. 2016. Sensory input attenuation allows predictive sexual response in yeast. *Nat Commun*. 7:12590.

Baryshnikova, A., M. Costanzo, S. Dixon, F.J. Vizeacoumar, C.L. Myers, B. Andrews, and C. Boone. 2010. Synthetic genetic array (SGA) analysis in Saccharomyces cerevisiae and Schizosaccharomyces pombe. *Methods Enzymol*. 470:145-179.

Bodenmiller, B., S. Wanka, C. Kraft, J. Urban, D. Campbell, P.G. Pedrioli, B. Gerrits, P. Picotti, H. Lam, O. Vitek, M.Y. Brusniak, B. Roschitzki, C. Zhang, K.M. Shokat, R. Schlapbach, A. Colman-Lerner, G.P. Nolan, A.I. Nesvizhskii, M. Peter, R. Loewith, C. von Mering, and R. Aebersold. 2010. Phosphoproteomic analysis reveals interconnected system-wide responses to perturbations of kinases and phosphatases in yeast. *Sci Signal*. 3:rs4.

Brachmann, C.B., A. Davies, G.J. Cost, E. Caputo, J. Li, P. Hieter, and J.D. Boeke. 1998. Designer deletion strains derived from Saccharomyces cerevisiae S288C: a useful set of strains and plasmids for PCR-mediated gene disruption and other applications. *Yeast*. 14:115-132.

Breslow, D.K., D.M. Cameron, S.R. Collins, M. Schuldiner, J. Stewart-Ornstein, H.W. Newman, S. Braun, H.D. Madhani, N.J. Krogan, and J.S. Weissman. 2008. A comprehensive strategy enabling high-resolution functional analysis of the yeast genome. *Nature Methods*. 5:711-718.

Butty, A.C., P.M. Pryciak, L.S. Huang, I. Herskowitz, and M. Peter. 1998. The role of Far1p in linking the heterotrimeric G protein to polarity establishment proteins during yeast mating. *Science*. 282:1511-1516.

Chen, W., Q. Nie, T.M. Yi, and C.S. Chou. 2016. Modelling of Yeast Mating Reveals Robustness Strategies for Cell-Cell Interactions. *PLoS Comput Biol*. 12:e1004988.

Choudhury, S., P. Baradaran-Mashinchi, and M.P. Torres. 2018. Negative Feedback Phosphorylation of Ggamma Subunit Ste18 and the Ste5 Scaffold Synergistically Regulates MAPK Activation in Yeast. *Cell Rep*. 23:1504-1515.

Chymkowitch, P., V. Eldholm, S. Lorenz, C. Zimmermann, J.M. Lindvall, M. Bjoras, L.A. Meza-Zepeda, and J.M. Enserink. 2012. Cdc28 kinase activity regulates the basal transcription machinery at a subset of genes. *Proc Natl Acad Sci U S A*. 109:10450-10455.

Chymkowitch, P., P.A. Nguea, H. Aanes, J. Robertson, A. Klungland, and J.M. Enserink. 2017. TORC1-dependent sumoylation of Rpc82 promotes RNA polymerase III assembly and activity. *Proc Natl Acad Sci U S A*. 114:1039-1044.

Colman-Lerner, A., A. Gordon, E. Serra, T. Chin, O. Resnekov, D. Endy, C.G. Pesce, and R. Brent. 2005. Regulated cell-to-cell variation in a cell-fate decision system. *Nature*. 437:699-706.

de Matos Simoes, R., S. Tripathi, and F. Emmert-Streib. 2012. Organizational structure and the periphery of the gene regulatory network in B-cell lymphoma. *BMC Syst Biol*. 6:38.

Dixit, G., J.B. Kelley, J.R. Houser, T.C. Elston, and H.G. Dohlman. 2014a. Cellular Noise Suppression by the Regulator of G Protein Signaling Sst2. *Molecular Cell*. 55:85-96.

Dixit, G., J.B. Kelley, J.R. Houser, T.C. Elston, and H.G. Dohlman. 2014b. Cellular noise suppression by the regulator of G protein signaling Sst2. *Mol Cell*. 55:85-96.

Dohlman, H.G., D. Apaniesk, Y. Chen, J.P. Song, and D. Nusskern. 1995. Inhibition of G-Protein Signaling by Dominant Gain-of-Function Mutations in Sst2p, a Pheromone Desensitization Factor in Saccharomyces-Cerevisiae. *Molecular and Cellular Biology*. 15:3635-3643.

Dohlman, H.G., J.P. Song, D.R. Ma, W.E. Courchesne, and J. Thorner. 1996. Sst2, a negative regulator of pheromone signaling in the yeast Saccharomyces cerevisiae: Expression, localization, and genetic interaction and physical association with Gpa1 (the G-protein alpha subunit). *Molecular and Cellular Biology*. 16:5194-5209.

Edelstein, A., N. Amodaj, K. Hoover, R. Vale, and N. Stuurman. 2010. Computer control of microscopes using microManager. *Curr Protoc Mol Biol*. Chapter 14:Unit14 20.

Eling, N., M.D. Morgan, and J.C. Marioni. 2019. Challenges in measuring and understanding biological noise. *Nat Rev Genet*. 20:536-548.

Elion, E.A., B. Satterberg, and J.E. Kranz. 1993. FUS3 phosphorylates multiple components of the mating signal transduction cascade: evidence for STE12 and FAR1. *Mol Biol Cell*. 4:495-510.

Ferrell, J.E., Jr. 2002. Self-perpetuating states in signal transduction: positive feedback, double-negative feedback and bistability. *Curr Opin Cell Biol*. 14:140-148.

Flores-Rozas, H., and R.D. Kolodner. 1998. The Saccharomyces cerevisiae MLH3 gene functions in MSH3-dependent suppression of frameshift mutations. *Proc Natl Acad Sci U S A*. 95:12404-12409.

Giaever, G., A.M. Chu, L. Ni, C. Connelly, L. Riles, S. Veronneau, S. Dow, A. Lucau-Danila, K. Anderson, B. Andre, A.P. Arkin, A. Astromoff, M. El Bakkoury, R. Bangham, R. Benito, S. Brachat, S. Campanaro, M. Curtiss, K. Davis, A. Deutschbauer, K.D. Entian, P. Flaherty, F. Foury, D.J. Garfinkel, M. Gerstein, D. Gotte, U. Guldener, J.H. Hegemann, S. Hempel, Z. Herman, D.F. Jaramillo, D.E. Kelly, S.L. Kelly, P. Kotter, D. LaBonte, D.C. Lamb, N. Lan, H. Liang, H. Liao, L. Liu, C.Y. Luo, M. Lussier, R. Mao, P. Menard, S.L. Ooi, J.L. Revuelta, C.J. Roberts, M. Rose, P. Ross-Macdonald, B. Scherens, G. Schimmack, B. Shafer, D.D. Shoemaker, S. Sookhai-Mahadeo, R.K. Storms, J.N. Strathern, G. Valle, M. Voet, G. Volckaert, C.Y. Wang, T.R. Ward, J. Wilhelmy, E.A. Winzeler, Y.H. Yang, G. Yen, E. Youngman, K.X. Yu, H. Bussey, J.D. Boeke, M. Snyder, P. Philippsen, R.W. Davis, and M. Johnston. 2002. Functional profiling of the Saccharomyces cerevisiae genome. *Nature*. 418:387-391.

Gnad, F., L.M. de Godoy, J. Cox, N. Neuhauser, S. Ren, J.V. Olsen, and M. Mann. 2009. High-accuracy identification and bioinformatic analysis of in vivo protein phosphorylation sites in yeast. *Proteomics*. 9:4642-4652.

Gould, C.J., M. Chesarone-Cataldo, S.L. Alioto, B. Salin, I. Sagot, and B.L. Goode. 2014. Saccharomyces cerevisiae Kelch proteins and Bud14 protein form a stable 520-kDa formin regulatory complex that controls actin cable assembly and cell morphogenesis. *J Biol Chem*. 289:18290-18301.

Helbig, A.O., S. Rosati, P.W. Pijnappel, B. van Breukelen, M.H. Timmers, S. Mohammed, M. Slijper, and A.J. Heck. 2010. Perturbation of the yeast N-acetyltransferase NatB induces elevation of protein phosphorylation levels. *BMC Genomics*. 11:685.

Herrera, M.C., P. Chymkowitch, J.M. Robertson, J. Eriksson, S.O. Boe, I. Alseth, and J.M. Enserink. 2018. Cdk1 gates cell cycle-dependent tRNA synthesis by regulating RNA polymerase III activity. *Nucleic Acids Res*. 46:11698-11711.

Hilfinger, A., and J. Paulsson. 2011. Separating intrinsic from extrinsic fluctuations in dynamic biological systems. *Proceedings of the National Academy of Sciences*. 108:12167-12172.

Holt, L.J., B.B. Tuch, J. Villen, A.D. Johnson, S.P. Gygi, and D.O. Morgan. 2009. Global analysis of Cdk1 substrate phosphorylation sites provides insights into evolution. *Science*. 325:1682-1686.

Howell, A.S., M. Jin, C.F. Wu, T.R. Zyla, T.C. Elston, and D.J. Lew. 2012. Negative feedback enhances robustness in the yeast polarity establishment circuit. *Cell*. 149:322-333.

Iida, H., Y. Yagawa, and Y. Anraku. 1990. Essential role for induced Ca2+ influx followed by [Ca2+]i rise in maintaining viability of yeast cells late in the mating pheromone response pathway. A

study of [Ca2+]i in single Saccharomyces cerevisiae cells with imaging of fura-2. *J Biol Chem*. 265:13391-13399.

Janke, C., M.M. Magiera, N. Rathfelder, C. Taxis, S. Reber, H. Maekawa, A. Moreno-Borchart, G. Doenges, E. Schwob, E. Schiebel, and M. Knop. 2004. A versatile toolbox for PCR-based tagging of yeast genes: new fluorescent proteins, more markers and promoter substitution cassettes. *Yeast*. 21:947-962.

Kaern, M., T.C. Elston, W.J. Blake, and J.J. Collins. 2005. Stochasticity in gene expression: from theories to phenotypes. *Nat Rev Genet*. 6:451-464.

Kinoshita, E., E. Kinoshita-Kikuta, K. Takiyama, and T. Koike. 2006. Phosphate-binding tag, a new tool to visualize phosphorylated proteins. *Molecular & Cellular Proteomics*. 5:749-757.

Lehner, B. 2008. Selection to minimise noise in living systems and its implications for the evolution of gene expression. *Mol Syst Biol*. 4:170.

Li, X., S.A. Gerber, A.D. Rudner, S.A. Beausoleil, W. Haas, J. Villen, J.E. Elias, and S.P. Gygi. 2007. Large-scale phosphorylation analysis of alpha-factor-arrested Saccharomyces cerevisiae. *J Proteome Res*. 6:1190-1197.

Malleshaiah, M.K., V. Shahrezaei, P.S. Swain, and S.W. Michnick. 2010. The scaffold protein Ste5 directly controls a switch-like mating decision in yeast. *Nature*. 465:101-105.

Metzger, B.P., D.C. Yuan, J.D. Gruber, F. Duveau, and P.J. Wittkopp. 2015. Selection on noise constrains variation in a eukaryotic promoter. *Nature*. 521:344-347.

Nern, A., and R.A. Arkowitz. 1999. A Cdc24p-Far1p-Gbetagamma protein complex required for yeast orientation during mating. *J Cell Biol*. 144:1187-1202.

Oehlen, L.J.W.M., J.D. McKinney, and F.R. Cross. 1996. Ste12 and Mcm1 regulate cell cycle-dependent transcription of FAR1. *Molecular and Cellular Biology*. 16:2830-2837.

Paleologou, K.E., A.W. Schmid, C.C. Rospigliosi, H.Y. Kim, G.R. Lamberto, R.A. Fredenburg, P.T. Lansbury, Jr., C.O. Fernandez, D. Eliezer, M. Zweckstetter, and H.A. Lashuel. 2008. Phosphorylation at Ser-129 but not the phosphomimics S129E/D inhibits the fibrillation of alpha-synuclein. *J Biol Chem*. 283:16895-16905.

Paliwal, S., P.A. Iglesias, K. Campbell, Z. Hilioti, A. Groisman, and A. Levchenko. 2007. MAPK-mediated bimodal gene expression and adaptive gradient sensing in yeast. *Nature*. 446:46-51.

Philips, J., and I. Herskowitz. 1998. Identification of Kel1p, a kelch domain-containing protein involved in cell fusion and morphology in Saccharomyces cerevisiae. *J Cell Biol*. 143:375-389.

Pryciak, P.M., and F.A. Huntress. 1998. Membrane recruitment of the kinase cascade scaffold protein Ste5 by the Gbetagamma complex underlies activation of the yeast pheromone response pathway. *Genes Dev*. 12:2684-2697.

Raser, J.M., and E.K. O'Shea. 2005. Noise in gene expression: origins, consequences, and control. *Science*. 309:2010-2013.

Repetto, M.V., M.J. Winters, A. Bush, W. Reiter, D.M. Hollenstein, G. Ammerer, P.M. Pryciak, and A. Colman-Lerner. 2018. CDK and MAPK Synergistically Regulate Signaling Dynamics via a Shared Multi-site Phosphorylation Region on the Scaffold Protein Ste5. *Mol Cell*. 69:938-952 e936.

Roberts, C.J., B. Nelson, M.J. Marton, R. Stoughton, M.R. Meyer, H.A. Bennett, Y.D. He, H. Dai, W.L. Walker, T.R. Hughes, M. Tyers, C. Boone, and S.H. Friend. 2000. Signaling and circuitry of multiple MAPK pathways revealed by a matrix of global gene expression profiles. *Science*. 287:873-880.

Schindelin, J., I. Arganda-Carreras, E. Frise, V. Kaynig, M. Longair, T. Pietzsch, S. Preibisch, C. Rueden, S. Saalfeld, B. Schmid, J.Y. Tinevez, D.J. White, V. Hartenstein, K. Eliceiri, P. Tomancak, and A. Cardona. 2012. Fiji: an open-source platform for biological-image analysis. *Nat Methods*. 9:676-682.

Severin, F.F., and A.A. Hyman. 2002. Pheromone induces programmed cell death in S. cerevisiae. *Curr Biol*. 12:R233-235.

Shaner, N.C., G.G. Lambert, A. Chammas, Y. Ni, P.J. Cranfill, M.A. Baird, B.R. Sell, J.R. Allen, R.N. Day, M. Israelsson, M.W. Davidson, and J. Wang. 2013. A bright monomeric green fluorescent protein derived from Branchiostoma lanceolatum. *Nat Methods*. 10:407-409.

Siekhaus, D.E., and D.G. Drubin. 2003. Spontaneous receptor-independent heterotrimeric G-protein signalling in an RGS mutant. *Nat Cell Biol*. 5:231-235.

Smolka, M.B., C.P. Albuquerque, S.H. Chen, and H. Zhou. 2007. Proteome-wide identification of in vivo targets of DNA damage checkpoint kinases. *Proc Natl Acad Sci U S A*. 104:10364-10369.

Tong, A.H., M. Evangelista, A.B. Parsons, H. Xu, G.D. Bader, N. Page, M. Robinson, S. Raghibizadeh, C.W. Hogue, H. Bussey, B. Andrews, M. Tyers, and C. Boone. 2001a. Systematic genetic analysis with ordered arrays of yeast deletion mutants. *Science*. 294:2364-2368.

Tong, A.H.Y., M. Evangelista, A.B. Parsons, H. Xu, G.D. Bader, N. Page, M. Robinson, S. Raghibizadeh, C.W.V. Hogue, H. Bussey, B. Andrews, M. Tyers, and C. Boone. 2001b. Systematic genetic analysis with ordered arrays of yeast deletion mutants. *Science*. 294:2364-2368.

van Drogen, F., R. Mishra, F. Rudolf, M.J. Walczak, S.S. Lee, W. Reiter, B. Hegemann, S. Pelet, I. Dohnal, A. Binolfi, Z. Yudina, P. Selenko, G. Wider, G. Ammerer, and M. Peter. 2019. Mechanical stress impairs pheromone signaling via Pkc1-mediated regulation of the MAPK scaffold Ste5. *J Cell Biol*. 218:3117-3133.

Volfson, D., J. Marciniak, W.J. Blake, N. Ostroff, L.S. Tsimring, and J. Hasty. 2006. Origins of extrinsic variability in eukaryotic gene expression. *Nature*. 439:861-864.

Wagih, O., M. Usaj, A. Baryshnikova, B. VanderSluis, E. Kuzmin, M. Costanzo, C.L. Myers, B.J. Andrews, C.M. Boone, and L. Parts. 2013. SGAtools: one-stop analysis and visualization of array-based genetic interaction screens. *Nucleic Acids Res*. 41:W591-596.

Wang, Z., and J. Zhang. 2011. Impact of gene expression noise on organismal fitness and the efficacy of natural selection. *Proc Natl Acad Sci U S A*. 108:E67-76.

Yu, R.C., C.G. Pesce, A. Colman-Lerner, L. Lok, D. Pincus, E. Serra, M. Holl, K. Benjamin, A. Gordon, and R. Brent. 2008. Negative feedback that improves information transmission in yeast signalling. *Nature*. 456:755-761.

Zhang, N.N., D.D. Dudgeon, S. Paliwal, A. Levchenko, E. Grote, and K.W. Cunningham. 2006. Multiple signaling pathways regulate yeast cell death during the response to mating pheromones. *Mol Biol Cell*. 17:3409-3422.

Figure 1

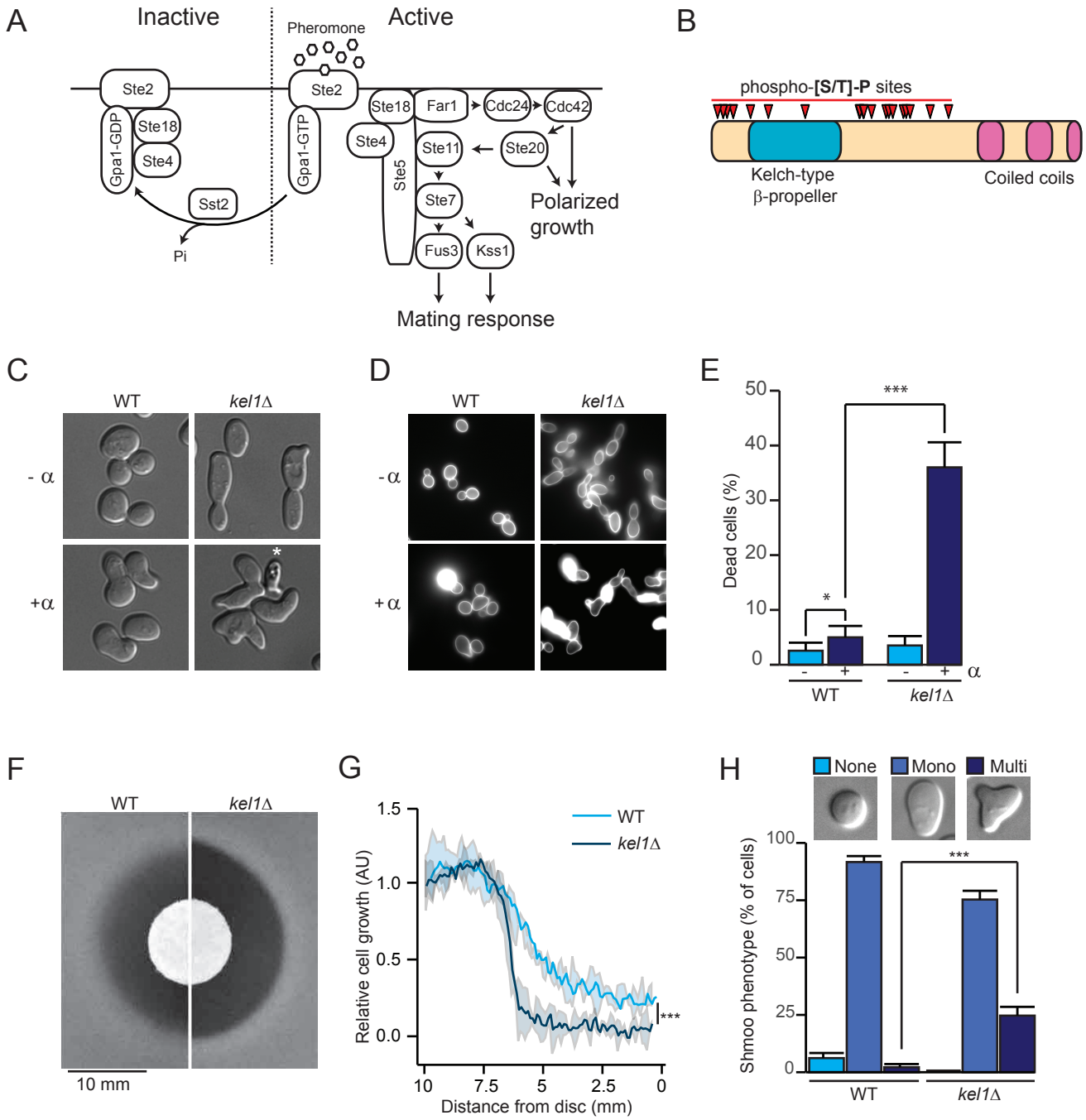
A
Inactive
Active
Pheromone
Ste2
Gpa1-GDP
Ste18
Ste4
Sst2
Pi
Gpa1-GTP
Ste5
Far1
Cdc24
Cdc42
Ste11
Ste20
Ste7
Fus3
Kss1
Polarized growth
Mating response
B
phospho-[S/T]-P sites
Kelch-type β-propeller
Coiled coils
C
WT
kel1Δ
- α
+α
D
WT
kel1Δ
- α
+ α
E
Dead cells (%)
50
40
30
20
10
0
***
*
- +
- +
α
WT
kel1Δ
F
WT
kel1Δ
10 mm
G
Relative cell growth (AU)
1.5
1.0
0.5
0.0
WT
kel1Δ
***
10
7.5
5
2.5
0
Distance from disc (mm)
H
None
Mono
Multi
Shmoo phenotype (% of cells)
100
75
50
25
0
***
WT
kel1Δ

Figure 2

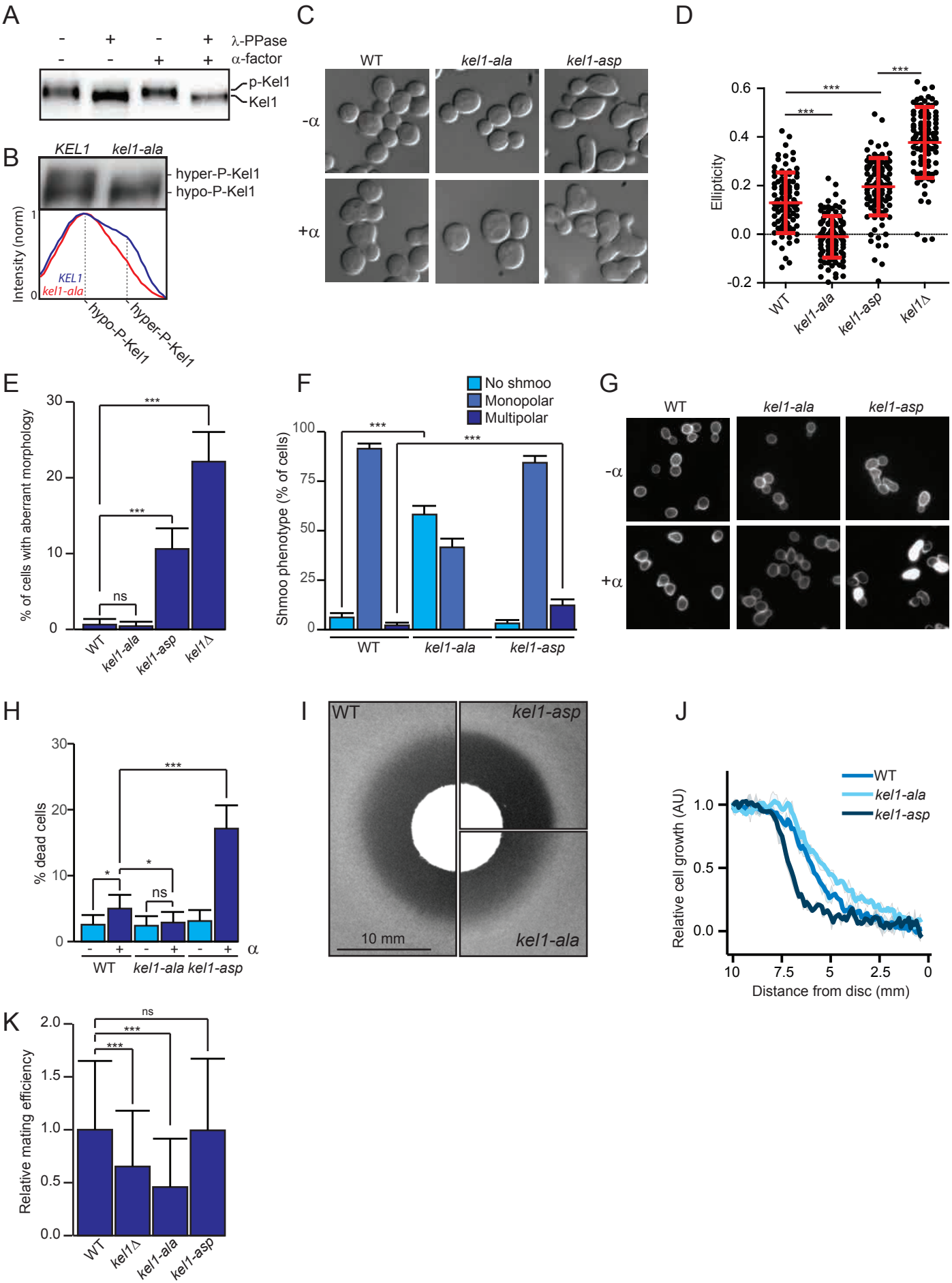
A
λ-PPase
α-factor
p-Kel1
Kel1
B
KEL1
kel1-ala
hyper-P-Kel1
hypo-P-Kel1
Intensity (norm)
C
WT
kel1-ala
kel1-asp
-α
+α
D
Ellipticity
WT
kel1-ala
kel1-asp
kel1Δ
E
% of cells with aberrant morphology
ns
F
No shmoo
Monopolar
Multipolar
Shmoo phenotype (% of cells)
G
H
% dead cells
I
10 mm
J
Relative cell growth (AU)
Distance from disc (mm)
K
Relative mating efficiency

Figure 3

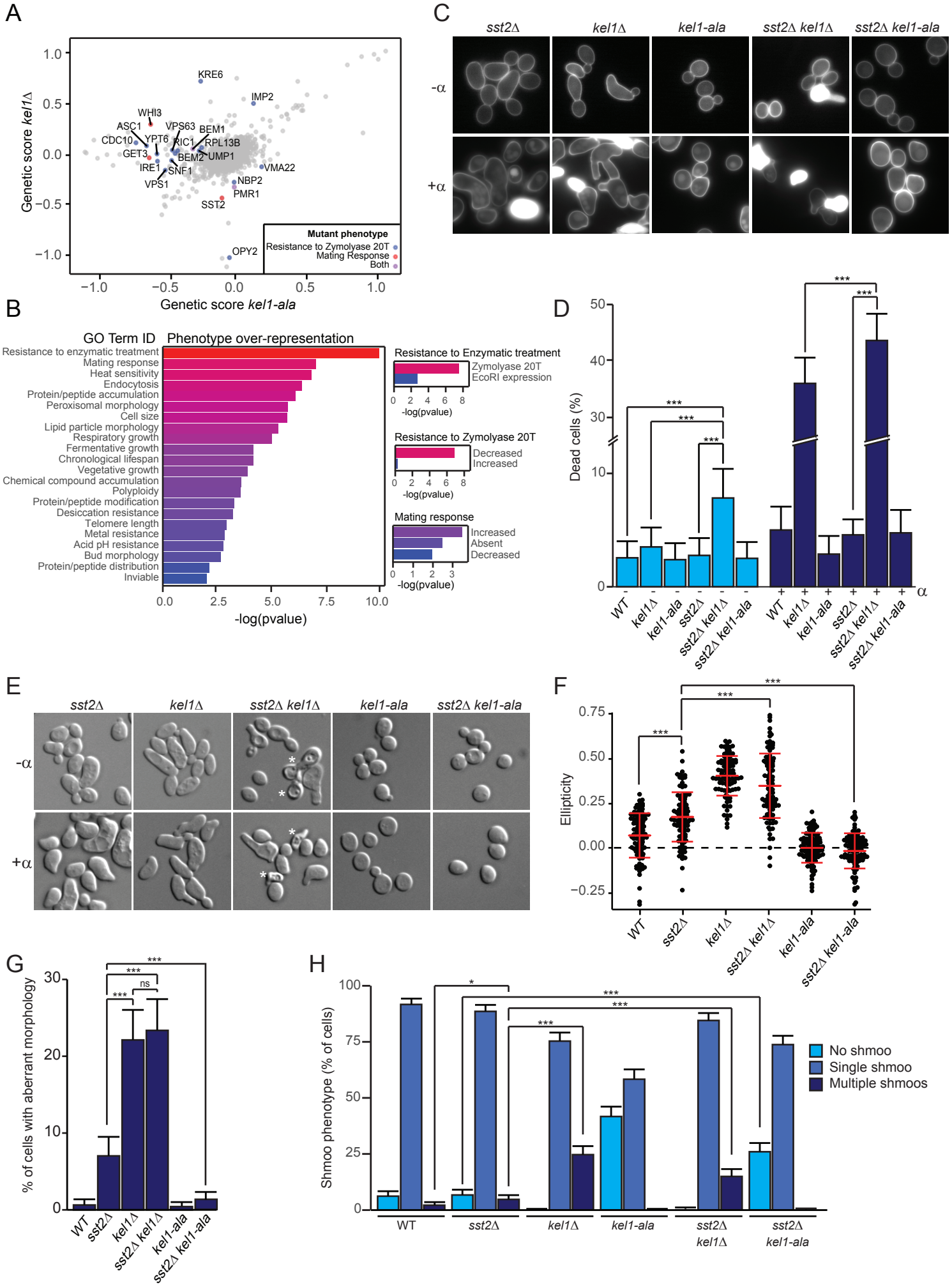
A
Genetic score kel1Δ
Genetic score kel1-ala
KRE6
IMP2
WHI3
ASC1
VPS63
BEM1
CDC10
YPT6
RIC1
RPL13B
GET3
BEM2
UMP1
IRE1
SNF1
VMA22
VPS1
NBP2
PMR1
SST2
OPY2
Mutant phenotype
Resistance to Zymolyase 20T
Mating Response
Both
B
GO Term ID
Phenotype over-representation
Resistance to enzymatic treatment
Mating response
Heat sensitivity
Endocytosis
Protein/peptide accumulation
Peroxisomal morphology
Cell size
Lipid particle morphology
Respiratory growth
Fermentative growth
Chronological lifespan
Vegetative growth
Chemical compound accumulation
Polyploidy
Protein/peptide modification
Desiccation resistance
Telomere length
Metal resistance
Acid pH resistance
Bud morphology
Protein/peptide distribution
Inviable
-log(pvalue)
Resistance to Enzymatic treatment
Zymolyase 20T
EcoRI expression
Resistance to Zymolyase 20T
Decreased
Increased
Mating response
Increased
Absent
Decreased
C
sst2Δ
kel1Δ
kel1-ala
sst2Δ kel1Δ
sst2Δ kel1-ala
-α
+α
D
Dead cells (%)
WT
kel1Δ
kel1-ala
sst2Δ
sst2Δ kel1Δ
sst2Δ kel1-ala
α
E
sst2Δ
kel1Δ
sst2Δ kel1Δ
kel1-ala
sst2Δ kel1-ala
-α
+α
F
Ellipticity
WT
sst2Δ
kel1Δ
sst2Δ kel1Δ
kel1-ala
sst2Δ kel1-ala
G
% of cells with aberrant morphology
ns
H
Shmoo phenotype (% of cells)
No shmoo
Single shmoo
Multiple shmoos
WT
sst2Δ
kel1Δ
kel1-ala
sst2Δ kel1Δ
sst2Δ kel1-ala

Figure 4

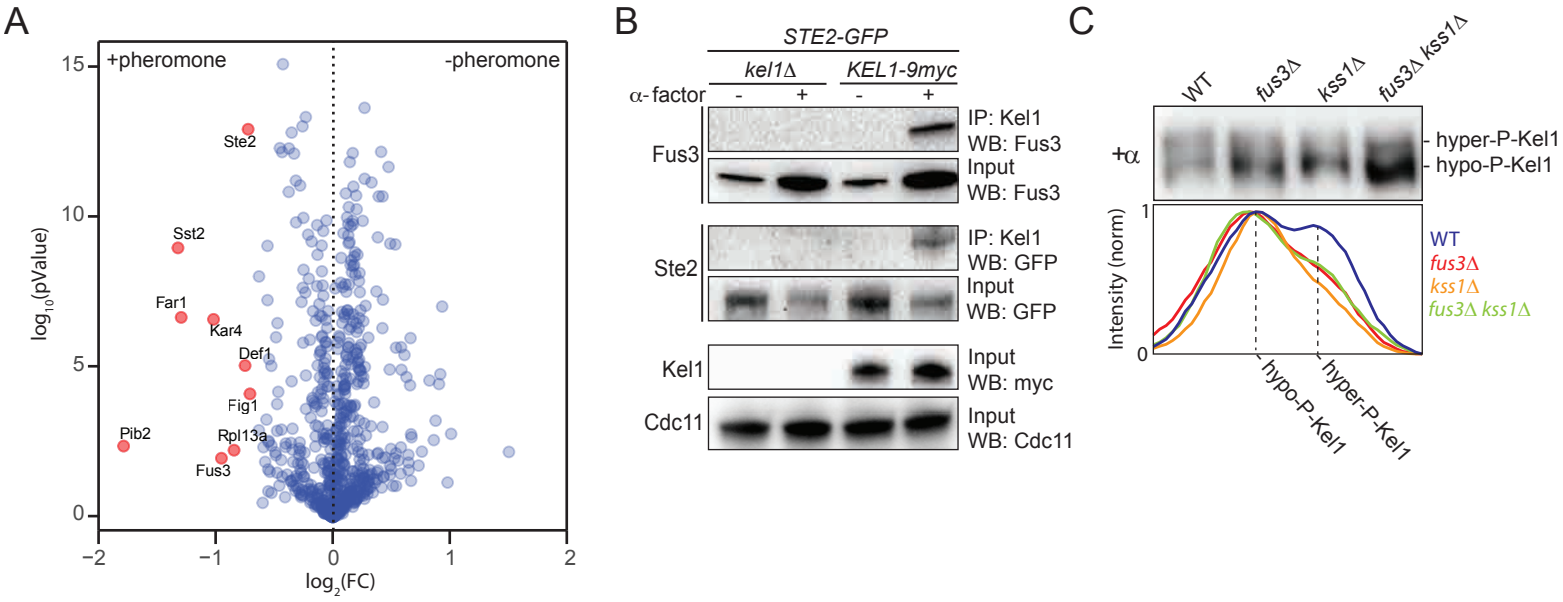
A
+pheromone
-pheromone
Ste2
Sst2
Far1
Kar4
Def1
Fig1
Pib2
Rpl13a
Fus3
log10(pValue)
log2(FC)
B
STE2-GFP
kel1Δ
KEL1-9myc
α-factor
-
+
-
+
Fus3
IP: Kel1
WB: Fus3
Input
WB: Fus3
Ste2
IP: Kel1
WB: GFP
Input
WB: GFP
Kel1
Input
WB: myc
Cdc11
Input
WB: Cdc11
C
WT
fus3Δ
kss1Δ
fus3Δ kss1Δ
+α
hyper-P-Kel1
hypo-P-Kel1
Intensity (norm)
WT
fus3Δ
kss1Δ
fus3Δ kss1Δ
hypo-P-Kel1
hyper-P-Kel1

Figure 5

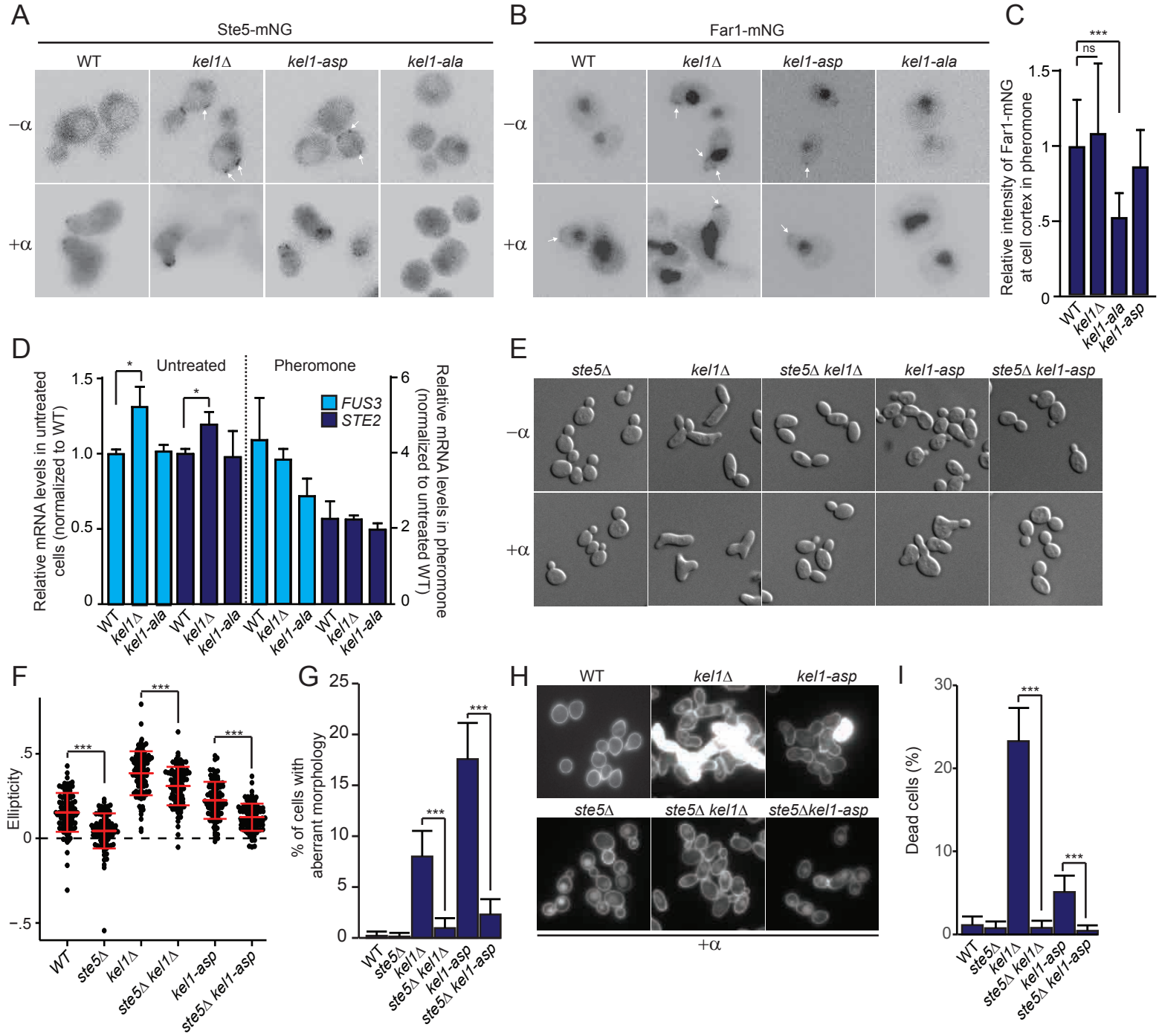
A
Ste5-mNG
WT
kel1Δ
kel1-asp
kel1-ala
−α
+α
B
Far1-mNG
WT
kel1Δ
kel1-asp
kel1-ala
−α
+α
C
***
ns
Relative intensity of Far1-mNG at cell cortex in pheromone
1.5
1
.5
0
WT
kel1Δ
kel1-ala
kel1-asp
D
Untreated
Pheromone
*
*
FUS3
STE2
Relative mRNA levels in untreated cells (normalized to WT)
Relative mRNA levels in pheromone (normalized to untreated WT)
1.5
1.0
0.5
0
6
4
2
0
WT
kel1Δ
kel1-ala
WT
kel1Δ
kel1-ala
WT
kel1Δ
kel1-ala
WT
kel1Δ
kel1-ala
E
ste5Δ
kel1Δ
ste5Δ kel1Δ
kel1-asp
ste5Δ kel1-asp
−α
+α
F
Ellipticity
.5
0
−.5
***
***
***
WT
ste5Δ
kel1Δ
ste5Δ kel1Δ
kel1-asp
ste5Δ kel1-asp
G
% of cells with aberrant morphology
25
20
15
10
5
0
***
***
WT
ste5Δ
kel1Δ
ste5Δ kel1Δ
kel1-asp
ste5Δ kel1-asp
H
WT
kel1Δ
kel1-asp
ste5Δ
ste5Δ kel1Δ
ste5Δkel1-asp
+α
I
Dead cells (%)
30
20
10
0
***
***
WT
ste5Δ
kel1Δ
ste5Δ kel1Δ
kel1-asp
ste5Δ kel1-asp

Figure 6

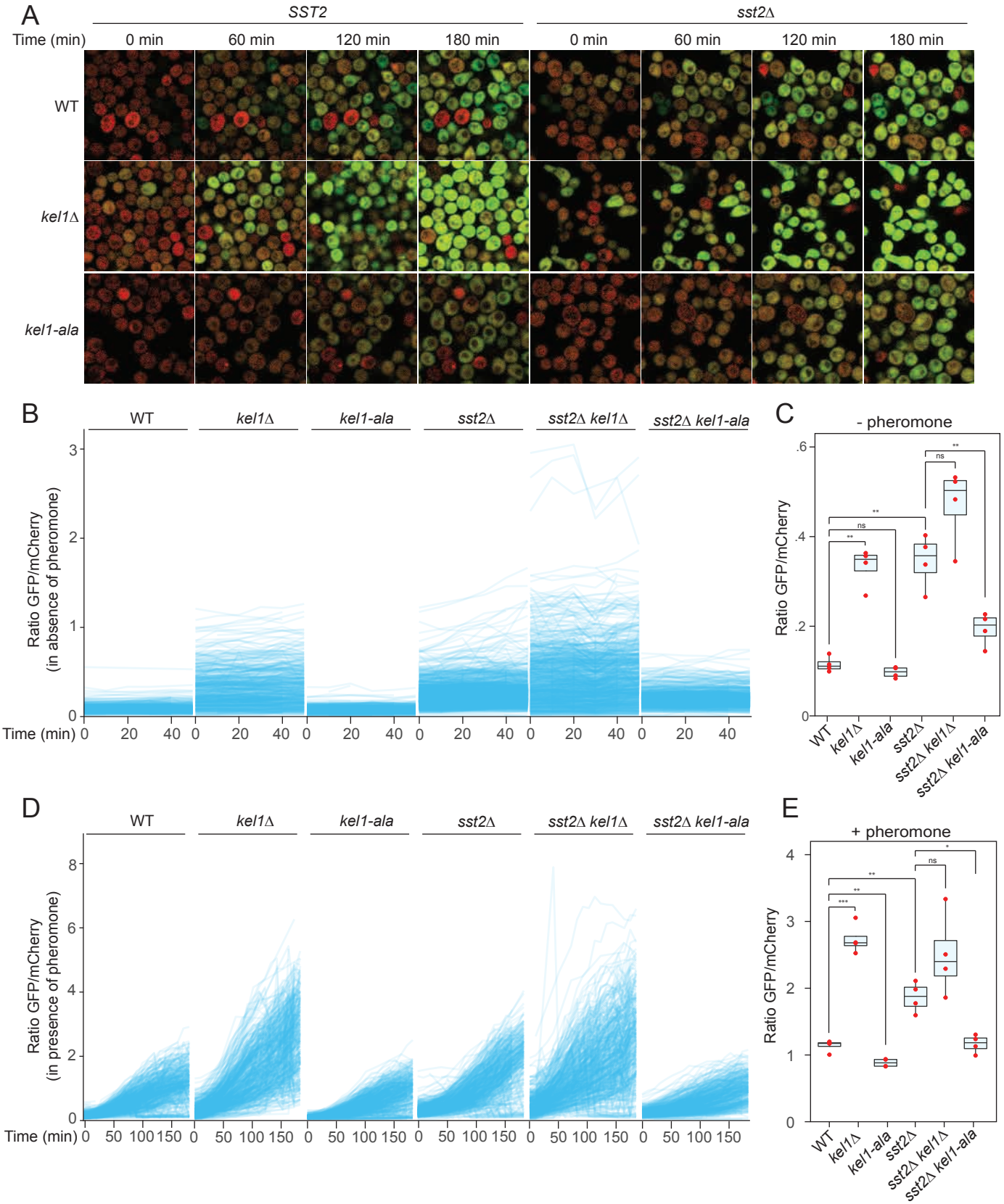
A
SST2
sst2Δ
Time (min)
0 min
60 min
120 min
180 min
WT
kel1Δ
kel1-ala
B
WT
kel1Δ
kel1-ala
sst2Δ
sst2Δ kel1Δ
sst2Δ kel1-ala
Ratio GFP/mCherry
(in absence of pheromone)
Time (min)
C
- pheromone
Ratio GFP/mCherry
D
Ratio GFP/mCherry
(in presence of pheromone)
E
+ pheromone
Ratio GFP/mCherry

Figure 7

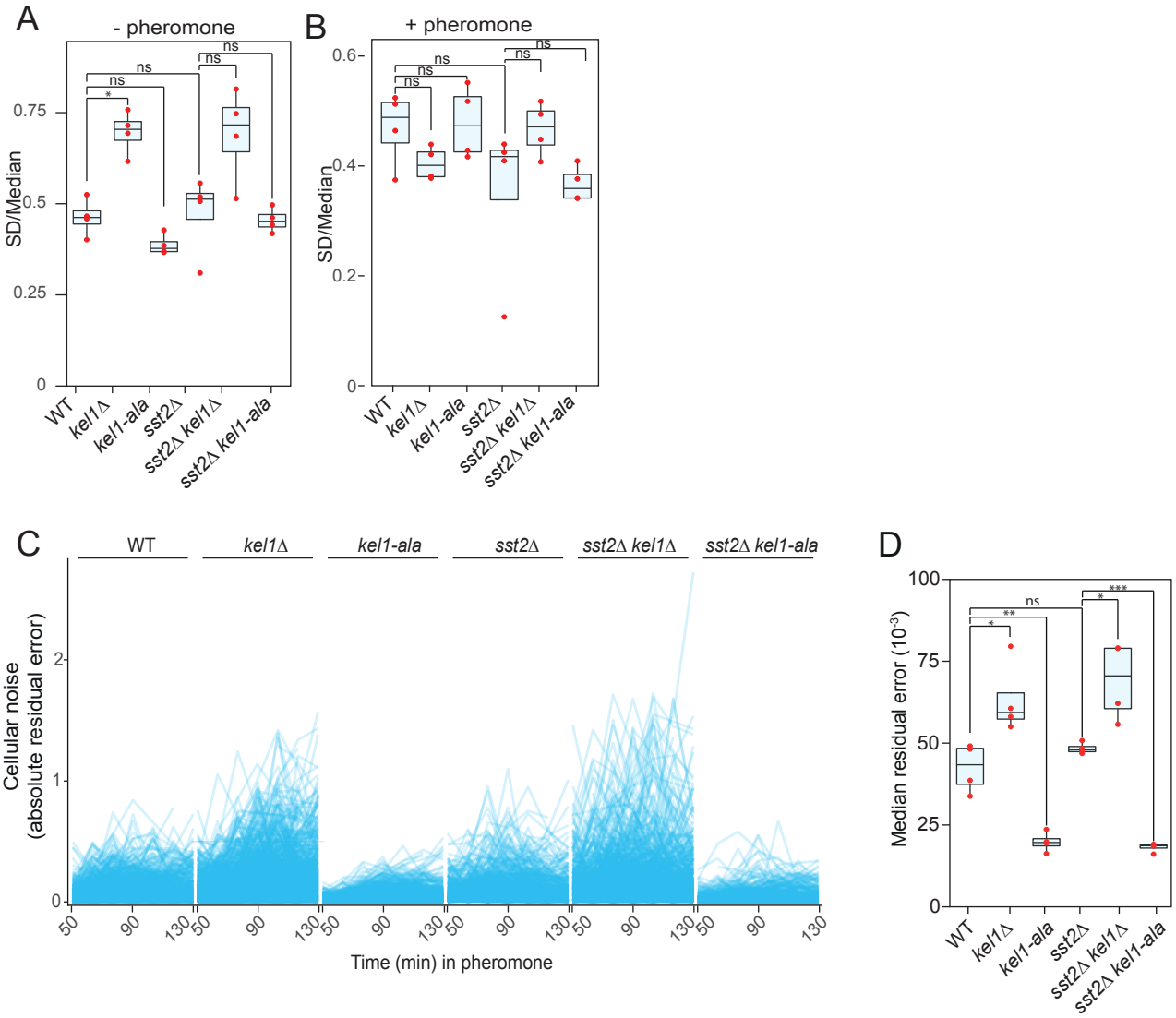
A
- pheromone
SD/Median
0
0.25
0.5
0.75
ns
ns
ns
ns
*
WT
kel1Δ
kel1-ala
sst2Δ
sst2Δ kel1Δ
sst2Δ kel1-ala
B
+ pheromone
SD/Median
0
0.2
0.4
0.6
ns
ns
ns
ns
ns
WT
kel1Δ
kel1-ala
sst2Δ
sst2Δ kel1Δ
sst2Δ kel1-ala
C
WT
kel1Δ
kel1-ala
sst2Δ
sst2Δ kel1Δ
sst2Δ kel1-ala
Cellular noise
(absolute residual error)
0
1
2
50
90
130
Time (min) in pheromone
D
Median residual error (10⁻³)
0
25
50
75
100
ns
**
*
*
***
WT
kel1Δ
kel1-ala
sst2Δ
sst2Δ kel1Δ
sst2Δ kel1-ala